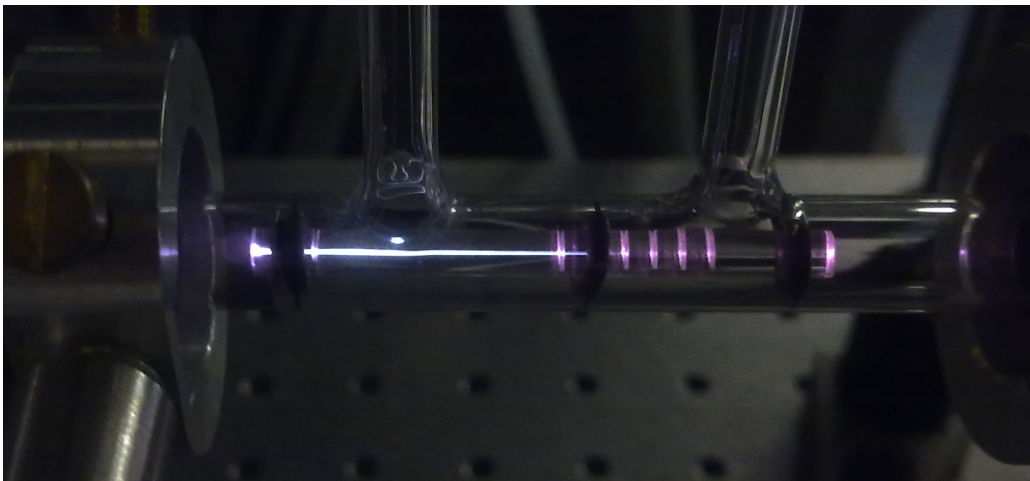MASTER OF PHYSICS AND PHOTONICS
INTERNSHIP REPORT

Coherent Control of High-Harmonic Generation

Supervisors:
Dr. Peter VAN DER SLOT
Author:
Jonathan BARREAUX
Dr. Bert BASTIAENS
Prof. Dr. Klaus BOLLER

LASER PHYSICS AND NONLINEAR OPTICS GROUP

MESA+ INSTITUTE FOR NANOTECHNOLOGY

FACULTY OF SCIENCE AND TECHNOLOGY

UNIVERSITY OF TWENTE

THE NETHERLANDS

August 27, 2012

Contents

List of Figures

Acknowledgment

The research described in this report was performed as the final part of the Master of Physics and Photonics from the Sciences and Properties of Matter education unit of the University of Rennes 1, France. Thanks to the Erasmus exchange program, it was made in the Laser Physics and Nonlinear Optics group of the University of Twente, The Netherlands. Working with this "double student identity" was a really great experience for me, for both my professional and personal skills. It allowed me to see further in the world of physics and to realize how important the sharing of the knowledges between people and laboratories is. During my stay, I only met wonderful people, always ready to help, share experience and give advices, and I am really proud today to continue the adventure in the LPNO group for the next four years as a PhD student.

First of all, I want to thank all my family, and more especially my parents, for all the support they gave to me in the execution of this project and for all the support that, I know, they will continue to give me in the future.

Then, I would like to thank Siew Jean Goh for teaching me how to work with the experimental set-up, showing me tricks for the alignment, discussing measurements and for all the time spent to fix the experiment before the deadline of my internship, and Yin Tao for all the advices he gave to me about the setup and the help when it was out of order.

Thanks to Fred van Goor for helping me with the autocorrelator and GRENOUILLE measurements, as well as for providing me the crystals for second harmonic generation.

I would like to thank Bert Bastiaens for his pertinent remarks and to make me think better about what I should do and how I should do it. Talking with you allowed me to learn to organize my thoughts and then to understand better my work.

I thank Peter van der Slot for supervising me and for revising my report. Even when you were really busy, you always took some minutes to help me about some theoretical or mathematical issues.

Thanks also to Klaus Boller for his very wise words, I learned a lot from the discussions we had together.

And finally, I would like to thank all the LPNO students for the very nice workdays we spent together, the fun times during the lunch breaks and the frisbee games we played when the weather was nice enough.

Coherent Control of High-Harmonic Generation

Introduction

High-harmonic generation (HHG) is a non-linear optical process that can convert laser light with standard wavelengths, such as infrared light, into coherent radiation at much shorter wavelengths in the XUV (extreme ultraviolet) or soft X-ray regime. As opposed to low-order nonlinear frequency conversion processes, such as second-harmonic generation, where moderate laser intensities are sufficient, high-order harmonics result from the highly nonlinear interaction of high-intensity laser pulses with typically a gaseous medium [1]. Ultrashort laser pulses of femtosecond duration are used for the generation of high-harmonics, focused to very high intensities ($\geq 10^{14}$ W/cm2) at a gaseous target. In the strong field present at the laser focus, electrons are ionized from the gas atoms. These electrons gain additional energy in the laser field and, upon recombination with the parent ion, emit harmonic XUV radiation. As the process of ionization and recombination takes place every half-cycle of the laser pulse, a spectrum of odd harmonics of the fundamental laser frequency is generated.

If sources based on HHG hold unique promises for a lot of applications (imaging, microscopy), it could be interesting to have the possibility to tune or enhance the produced discrete high-harmonics. This might allow an extension of the applications, like for instance the seeding of free-electron lasers (FEL), offering potentially a major improvement in the output performance. Main works on tuning or enhancement of high-harmonics are made by shaping of the drive lasers pulses, changing the spectral amplitude or phase.

In previous work performed by the Laser Physics & Nonlinear Optics (LPNO) group at the University of Twente, an experimental set-up for HHG was built and implemented, and high-harmonics were successfully produced and recorded [2, 3]. An acousto-optic programmable dispersive filter (AOPDF), which can shape an optical pulse by coupling it to an acoustic wave propagating inside a birefringent crystal, is placed immediately after the stretcher in the amplifier used for the generation of the high-intensity laser pulses. It allows to manipulate femtosecond pulses both in amplitude and phase at the same time.

This thesis is organized as follows. First, the theory of high harmonic generation is discussed in Chapter 1. It describes the two main aspects: the response of a single atom to the drive laser field and the coherent superposition of the harmonic radiations.

Next, the experimental set-up that is used to generate and characterize the high harmonics is described in Chapter 2. The process for the generation of high-harmonic is also explained here.

Chapter 3 describes the theory and use of the acousto-optic programmable dispersive filter (AOPDF), a device use for shaping of ultrashort pulses. A Matlab model of the AOPDF functions is also presented. Then the first attempts of tuning and enhancement of the high-harmonics using the AOPDF are discussed.

Finally, the conclusions of this work and an outlook for future research will be presented in the Summary.

Chapter 1

Theory of high-harmonic generation

In considering the generation of high harmonic radiation with high intensities, two main aspects can be distinguished. The response of a single atom to the drive laser field, the microscopic aspect, is described semi-classically in Section 1.1. The phase-matching conditions between the harmonic radiations from all atoms in the interaction volume, the macroscopic aspect, are described in Section 1.2.

1.1 Three-step model

The generation of high-harmonic radiations can be describe with a semi-classical model of a single-atom response, called the *three-step model* developed by Corkum [4] and depicted in Figure 1.1. A more complete, quantum mechanical model is necessary to also predict the phase and intensity of the radiation produced by a single atom. Such a model incorporates a solution to the three-dimensional Schrödinger equation describing the wave function of a single electron in the potential created by both its parent ion and the drive laser field [5]. This will, however, not be discussed in this report.
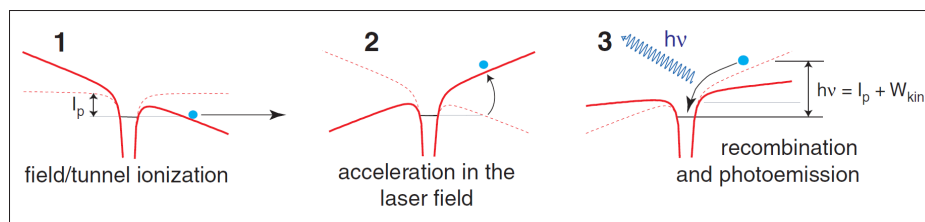
Figure 1.1: Illustration of the three-step model for high-harmonic generation: tunnel ionization of the electron (1), followed by acceleration in the laser electric field (2) and finally recombination and emission of a high-energy photon (3).

A single atom of the gaseous medium is considered. Exposed to the strong field of ultrashort high-intensity laser pulses, the shape of its Coulomb potential is modified. Typically, electric fields of at least 10^{11} V/m are applied. The outer-bound electron of this atom has then the possibility to escape the binding potential, by tunneling through or escaping over the lowered barrier. Now considered as a free and classical particle, it is accelerated away from its parent ion by the same electric field and follows a classical electron trajectory in a laser field. Finally, as soon as the oscillating electric field changes

direction, the electron is first decelerated and eventually reaches a point of zero velocity. From there it is accelerated back towards its parent ion. On its way back, the electron acquires again a large amount of kinetic energy due to the strong acceleration by the laser electric field.

The electron can recombine with its parent ion with a certain probability and emits a photon with a photon energy composed of the ionization energy of the atom I_p and the kinetic energy W_{kin} of the electron gained by its interaction with the laser field:

$$\hbar\omega = I_p + W_{kin}(\varphi) \tag{1.1}$$

Only photons with a photon energy of integer multiples of the fundamental photon energy are generated. Due to interference effects the even numbered harmonics are erased, only odd numbered harmonics survive.

The kinetic energy W_{kin} depends on the phase φ of the electric field at the instant of ionization. Electrons emitted at different phases φ experience different trajectories and can return to the core with different kinetic energies as shown in Figure 1.2. If the ionization occurs too early during an optical cycle, the electron is accelerated away and decelerated, but never return to its parent ion (trajectory e, $\varphi = -45°$). An electon ionizing at the peak value of the electric field, where most ionizations occur, returns to its parent ion but with zero kinetic energy (trajectory d, $\varphi = 0°$). The trajectories a ($\varphi = 45°$) and c ($\varphi = 3°$) correspond to the short and long trajectory, respectively, leading to the same final energy. The highest kinetic energy is obtained when ionization occurs when the drive laser field has a phase $\varphi \approx 17°$ (cut-off trajectory b).
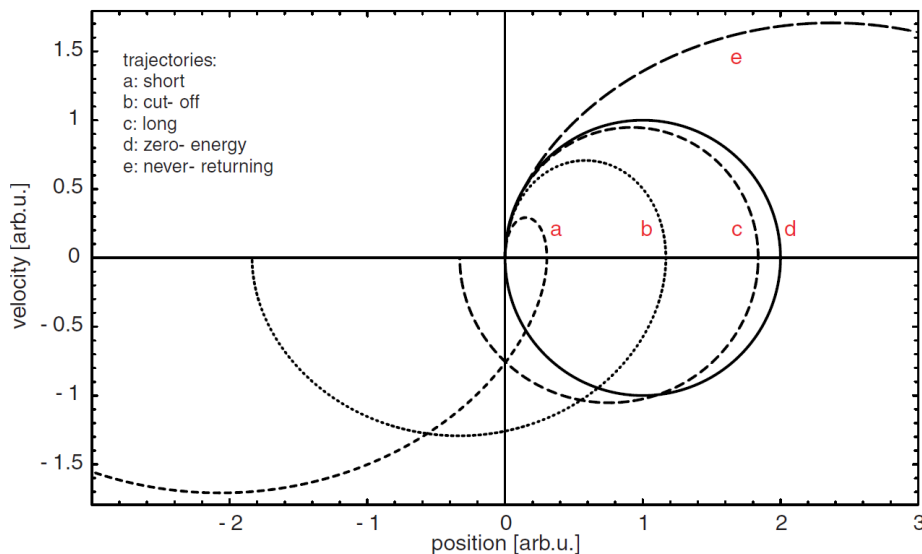
Figure 1.2: Different classes of electron trajectories during the propagation phase of high-harmonic generation, plotted in the position-velocity plane. The trajectories start at the atom located at $(0, 0)$.

The maximum kinetic energy of the electron upon its return to the core can be calculated using classical [4] or quantum mechanics [5] and is given by

$$W_{kin}^{max} = 3.17\frac{e^2 E_0^2}{4m_e\omega_0^2} = 3.17U_p \tag{1.2}$$

The kinetic energy is expressed in terms of the so-called ponderomotive energy U_p of the electron. It corresponds to the average quiver energy of an electron, having a mass

m_e and a charge e, in an oscillating laser field of amplitude E_0 and frequency ω_0. The ponderomotive energy is directly proportional to the intensity I_0 of the driving laser and the square of the fundamental wavelength λ_0:

$$U_p = \frac{e^2 E_0^2}{4 m_e \omega_0^2} \propto I_0 \lambda_0^2 \tag{1.3}$$

The maximum photon energy (cut-off energy) that can be achieved in this process is then given by

$$E_{cut-off} = \hbar \omega_{max} = I_p + 3.17 U_p, \tag{1.4}$$

This broad distribution of possible trajectories and kinetic energies lead to a characteristic spectrum for high-harmonic, as shown in Figure 1.3. As can be seen, the intensity of the orders drops quickly with increasing order, then stays approximately constant within the so-called high-harmonic plateau, and then rapidly falls off beyond the cut-off frequency.
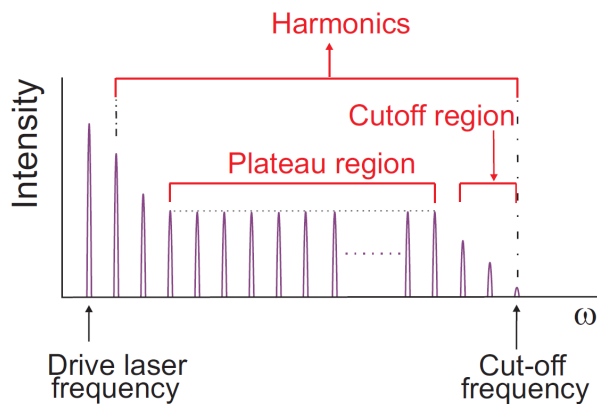
Figure 1.3: Typical high-harmonic spectrum.

According to Equations 1.2, 1.3 and 1.4, two options are available to increase the cut-off energy, that is, to obtain shorter wavelength radiation. Either a medium with a higher ionization potential I_p can be chosen, or the quiver energy can be increased. The latter is achieved by increasing either the drive laser intensity I_0 or the drive laser wavelength λ_0. Using a longer wavelength, greatly enlarges the cut-off energy through the contribution from the quiver energy, that scales with λ_0^2. However, the single atom response in the plateau region was found to decrease dramatically with a factor of $\lambda_0^{6.5}$ [6]. Therefore, using an increased drive laser intensity might be a more attractive option. The enhancement of the cut-off energy by either of these options is not investigated in this report.

1.2 Coherent superposition of harmonic radiations

The *three-step model*, which considers the individual response of single atoms, does not completely describe the high-harmonic generation process in a medium. For any nonlinear optical process to be efficient, the emission from a large number of atoms that are driven nonlinearly must radiate coherently. As the driving laser beam passes through the medium, a coherent harmonic signal builds-up that co-propagates with it. However, to build-up coherently over an extended propagation distance, the fundamental and harmonic beams must travel with the same phase velocity: the process must be phase matched. In a phase-matched frequency-conversion process, the nonlinear response from the medium

continues to add constructively to the signal beam, leading to a bright harmonic signal.

1.2.1 Phase-matching in a hollow waveguide

If the discrete nature of a typical high-harmonic spectrum, as shown in Figure 1.3, results from the periodicity of the laser electric field, the final height and shape of the spectrum are determined by phase matching. The phase matching condition is dependent on the shape of the interaction volume and on the spatio-temporal distribution of the drive laser field. As part of this work, we will focus on high-harmonic generation in a capillary. The use of a capillary presents two advantages: firstly the capillary can be considered as a hollow waveguide and secondly, it allows for phase matching by tuning the pressure of the gaseous medium.

The requirement for phase matching to increase the conversion efficiency is based on the following arguments. To get a considerable amount of output, the radiation emitted in the forward direction by each atom has to be in phase with the radiation emitted by the rest of the atoms. This is achieved when the phase velocity of the drive laser is equal to the phase velocity of the generated radiation. If this is not the case, for example for free propagation in a dispersive medium, the drive laser field slips out of phase with the generated radiation. In this case, after some characteristic propagation distance called the coherence length, the phase shift is π radians, and the newly generated radiation interferes destructively with the earlier generated radiation. This limits the generated radiation output to that from the coherence length, which is usually much less than the intended interaction length.

In order to see how phase matching can be established in a hollow waveguide consider the following. The wavevector of the fundamental drive laser light propagating through a hollow waveguide filled with a noble gas, which is possibly ionized to some degree, is given by [7, 8]:

$$k_f \approx \underbrace{\frac{2\pi}{\lambda}}_{\text{vacuum term}} + \underbrace{\frac{2\pi N_a n(\lambda)}{\lambda}}_{\text{neutral gas}} - \underbrace{N_e r_e \lambda}_{\text{plasma dispersion}} - \underbrace{\frac{u_{nm}^2 \lambda}{4\pi a^2}}_{\text{waveguide dispersion}} \tag{1.5}$$

where the first and the fourth term define together the wave vector for propagation in an empty hollow waveguide. The first term corresponds to simple vacuum propagation and the last term describes the correction to the vacuum propagation due to the presence of an empty waveguide, where a is the inner radius of the hollow waveguide and u_{nm} is the m$^{\text{th}}$ root of the Bessel function $J_{n-1}(z)$ for the waveguide (for the lowest order, $u_{11} = 2.405$), corresponding to the propagation mode in the capillary. The second and third term are corrections due to dispersion of the gas and of the plasma, respectively. Note that the contribution from the free electrons in the plasma is negative. Here, N_a is the instantaneous density of neutral atoms in the medium, $n(\lambda)$ is the linear refractive index per unit neutral atom density at the wavelength λ, N_e is the density of free electrons, and r_e is the classical electron radius.

In that same waveguide, according to Equation 1.5 and using $\lambda_q = \lambda/q$, the propagation vector of the q$^{\text{th}}$ harmonic beam is:

$$k_q = q \left(\frac{2\pi}{\lambda} + \frac{2\pi N_a n(\lambda_q)}{\lambda} - \frac{N_e r_e \lambda}{q^2} \right) \tag{1.6}$$

In this expression we neglected the waveguide term, because the high harmonic radiation

is usually emitted in a beam with low divergence, that is much smaller in diameter than the waveguide and hence does not interact with it.

The phase mismatch is then given by:

$$\Delta k_q = q k_f - k_q \tag{1.7}$$

or, by substituting with Equations 1.5 and 1.6 and assuming $\left(1 - 1/q^2\right) \approx 1 \; (q \gg 1)$:

$$\Delta k_q = q \left(P(1 - \eta)\Delta n_q \frac{2\pi}{\lambda} - P\eta N_0 r_e \lambda - \frac{u_{nm}^2 \lambda}{4\pi a^2} \right) \tag{1.8}$$

Here the particle densities have been substituted by the corresponding pressure, where η is the ionization fraction of the gas, P is the pressure in bar, N_0 is the particle density at 1 bar and $\Delta n_q \equiv n(\lambda) - n(\lambda_q)$ is the difference in refractive index of the gas at 1 bar between the fundamental wavelength λ and the high-order harmonic wavelength λ_q.

To obtain phase matching, and thus the highest harmonic conversion efficiency, the phase mismatch Δk_q has to be brought to zero. According to Equation 1.8, the first two terms are proportional to the pressure and for sufficiently small ionization fraction have a net positive contribution. Therefore, by tuning the pressure it can be made to compensate the negative contribution from the waveguide dispersion.

The second term, the dispersion of plasma, is determined by the plasma density, and thus by the degree of ionization of the gas. In particular, if this ionization is too large, the sum of the first two terms will be negative and the (negative) waveguide term can not be compensated. This means that there is a critical (maximum) ionization degree above which phase matching in a hollow waveguide is no longer possible by adjusting the pressure.

An estimate of the order of magnitude of the maximum ionization degree can be obtain by inserting typical parameters in Equation 1.8: it is typically of a few percent. For example, for Xenon, the critical ionization degree is 9 %, while for helium it is 0.6 %, assuming that the 41st harmonic of 800 nm radiation is to be generated in a waveguide of 150 μm diameter [2, 3].

Thus the current limits in high-harmonic generation, to reach short wavelengths in the nanometers regime, is given by ionization induced loss of phase matching when trying to increase the ponderomotive energy U_p (Equation 1.4) by increasing the drive laser intensity. Additionally, ionization lowers the density of the remaining neutral atoms and thus depletes the nonlinear response of the medium, which decreases the high-harmonic output as well.

1.2.2 Quasi-phase-matching

When phase matching by pressure tuning is not possible, because the ionization becomes too high, another approach, so-called quasi-phase matching, is of increased interest. The concept of this technique is also to only generate radiation that interferes constructively with the radiation already generated.

After a certain coherence length $L_c = \pi/\Delta k$, the second-harmonic field that is just being generated is out of phase by π with respect to the second-harmonic field generated first, leading to destructive interference between the two fields. The idea of quasi-phase matching is to invert the phase or diminish the amplitude of the generated high-harmonics at the sections where the drive beam is out of phase, until the drive beam is in phase with
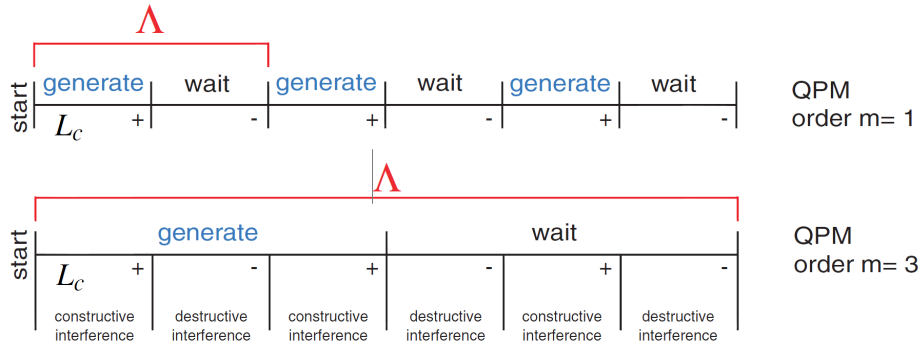
Figure 1.4: Scheme for quasi-phase matching. The nonlinear process takes place in the regions labeled *generate* while there is no nonlinear interaction in the *wait* regions (or of course generation of a "negative" signal). Signal generation always takes place along one coherence length L_c, so by introducing the *wait* regions we avoid destructive interference between the new and the old signal. The modulations periods for QPM with different orders (m) are denoted by Λ.

the harmonic wave again. The quasi-phase matching scheme is summarized in Figure 1.4. The signal is generated over the first coherence length. Instead of generating a signal of opposite sign in the second coherence length, we just wait, suspending signal generation. This process can be repeated periodically, leading to a stepwise build-up over the whole interaction region.

When using a non-centro-symmetric nonlinear crystal for example, the orientation of the crystal lattice can be changed periodically with the coherence length L_c, to achieve such phase inversion.

But in a gas, which is centro-symmetric, changing the orientation is not possible. Here, a periodic modulation of the amplitude of the harmonic generation is the approach of choice. This can for example be achieved by rapid axial intensity modulations caused by beating between the fundamental and higher-order modes in a waveguiding capillary, so that the intensity of the drive laser is lower in the out-of-phase sections. Another method could be to create a spatial modulation, at least transiently in a dynamic process, of the gas density along the waveguide.

In general, to obtain quasi-phase matching, we can introduce some modulation

$$\Lambda = \frac{2\pi m}{\Delta k} = 2mL_c \tag{1.9}$$

where m is the order of quasi-phase matching. If a modulation with a period of two coherence lengths is not possible, a modulation with an elongated period of $L = 2mL_c$ (where m is an odd integer) is also possible. For instance, as shown in Figure 1.4, with an order of quasi-phase matching $m = 3$, the signal is generated twice and destroyed once during the distance labeled *generate*, leaving a net gain.

Chapter 2

Experimental setup

There are several different configurations for the generation of high-harmonics. The main ones are the following: gas jet, gas cell, semi-infinite gas cell (SIGC) and hollow waveguide. These different configurations are represented in Figure 2.1.

In a gas jet setup, the drive laser is focussed into a gas jet with a width of typically a few millimeters. Typical conversion efficiencies obtain with these devices is 10^{-6}.

For the gas cell and the semi-infinite gas cell, the focusing is made into a glass cell of parallelepipedic shape filled with gas, enclosed by two windows for the gas cell and a single one for the semi-infinite gas cell. Windows are placed far away from the focus to limit nonlinear effects inside the window due to a high local field intensity. Typical interaction length and conversion efficiency are 13 mm and 5.10^{-5}, respectively, for the gas cell and 500 mm and 1.10^{-4}, respectively, for the semi-infinite gas cell.

Finally, the last configuration considered here is the hollow waveguide, and this is the configuration we use in our experiments. This configuration provides a typical conversion efficiency of 10^{-5} and an interaction length of a few centimeters.
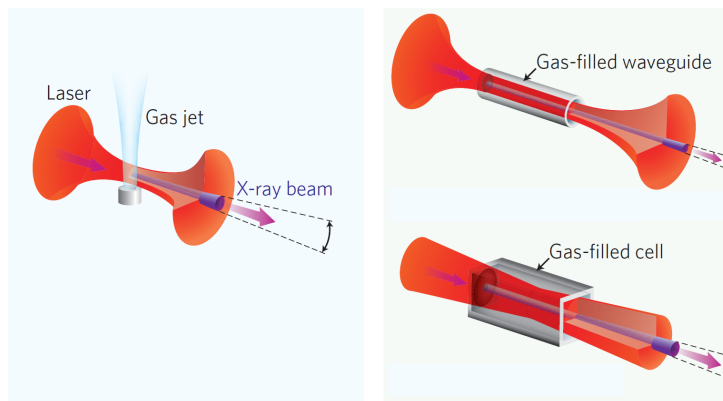
Figure 2.1: Main configurations for high-harmonic generation. Illustrations adapted from [9].

Our experimental setup (see Figure 2.2) for the generation of high-harmonic radiation can be subdivided into three parts, corresponding to the first three sections of this chapter.

First, generation of the strong laser field by a Ti:Sapphire oscillator coupled to an amplifier will be presented. The amplified ultrashort pulses have been characterized at the output of the amplifier using two methods: with an intensity autocorrelator and a GRENOUILLE. Furthermore, a Dazzler™ is mounted inside the amplifier. This device allows for pulse shaping and will be presented in Section 3.1.

The second part consists of the high-harmonic generation setup, which contains the capillary in which the strong laser field is focused and high-harmonics are generated.

The third part is the diagnostics section, which consists mainly of a XUV spectrometer used to characterize the generated radiation and composed of a thin aluminium filter to block the drive laser radiation, a grating and a XUV camera to image the generated radiation.

Finally, the last section of this chapter outlines the standard procedure for generation of high-harmonics.

2.1 Strong laser field source

The IR beam is provided by a mode-locked Ti:Sapphire laser oscillator (*Coherent Mantis^{TM}*), which produces broad-bandwidth pulses centered around 800 nm. The Ti:Sapphire crystal is pumped by a *Coherent OPS^{TM} (Optically Pumped Semiconductor)* pump laser. The oscillator itself employs Kerr-lens mode-locking in combination with negative dispersion mirrors to generate broad-bandwidth ultrafast pulses [10].

High-harmonic generation requires a very strong electric field, hence the IR pulses from the Ti:Sapphire oscillator have to be amplified. A *Coherent Legend Elite^{TM} Duo USP* amplifier is seeded by the *Coherent Mantis^{TM}* oscillator. According to the specifications provided in the manual, this setup allows amplification of pulses up to 8 mJ with a repetition rate of 1 kHz and a full-width at half-maximum of 40 fs [11].
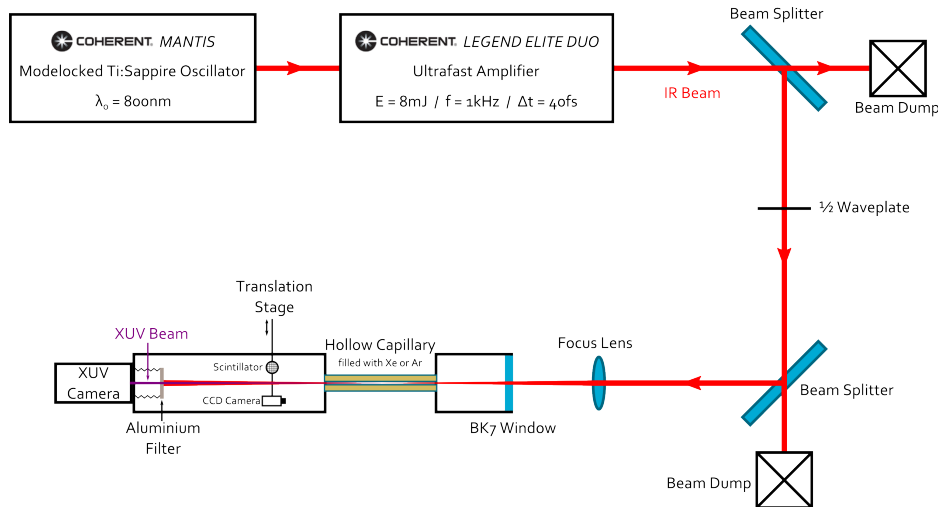
Figure 2.2: Simple sketch of our setup for HHG using a gas-filled hollow waveguide.

The pulse width at the output of the amplifier has been measured, using a high-resolution autocorrelator (*Femtochrome FR-103XL*) coupled with an oscilloscope. A complete profile, in time and frequency domain, of the ultrashort pulses was obtained using GRENOUILLE (*grating-eliminated no-nonsense observation of ultrafast incident laser light e-fields*), an enhancement of the FROG (*frequency-resolved optical gating*). This method is a spectrally resolved autocorrelation of ultrashort pulses, which allows the use of a phase-retrieval algorithm to retrieve the precise pulse intensity and phase as a function of time. It can measure both very simple and very complex ultrashort laser pulses, without the use of a reference pulse.

Only the most important results are presented here, more detailed informations about

the measurement processes for the autocorrelation and the GRENOUILLE can be found in the Appendix A. The width of the ultrashort pulses from the amplifier measured using the intensity autocorrelator is $\tau_{ac} \approx 46$ fs. Using the GRENOUILLE, the pulse width measured is $\tau_{GR} \approx 50$ fs and the bandwidth $\Delta\nu_{osc} \approx 9$ THz. These results are in a good agreement.

2.2 Hollow waveguide configuration

The capillary has a diameter of 150 μm and a length of a few cm. It can be filled with argon or xenon and the pressure is adjustable from 0 to 100 mbar. A translation stage positioned after the capillary allows to place either a scintillator or a mirror in the beam path of the generated EUV light. The mirror reflects the light directly to a CCD camera (*Pixelink PL-A741*). The beam profile of the drive laser field can be visualized with the CCD camera, in order to check for the proper matching to the hollow waveguide. The scintillator is used to check by eyes for the generation of high-harmonic. Indeed, when it is excited by XUV radiations, it emits a randomly directed blue fluorescence signal.

The capillary is mounted in vacuum, along with the scintillator, the mirror and the XUV spectrometer (introduced in the next section). This is to prevent defocusing of the focused infrared beam on the incouple side of the capillary and absorption of the generated high harmonics behind the capillary. A turbomolecular pump (coupled to a roughing pump to initialize the vacuum) is used and provides a high vacuum ($\sim 10^{-5}$ mbar).

The drive infrared beam is matched with the capillary using a lens with a focal length of 750 mm. A half-wave plate and two polarizing beam splitters are placed into the beam path and allow to adjust the power sent to the capillary. Before each experiment, the alignment of the capillary is checked using a He-Ne laser and the CCD camera placed after the capillary. Once the capillary is properly set, the drive laser beam can be injected. The matching of the drive laser beam to the capillary can also be verified using the CCD camera. The observed drive laser beam profile must be symmetric and intense and the plasma production in the capillary must be as low as possible. This is done by tweaking the focus lens, whose alignment might drift with the temperature in the laboratory, affecting the matching of the drive laser beam. Ideally the temperature should be constant to within 0.5 K.

2.3 XUV spectrometer

The spectrum of the generated high harmonics is measured with a simple spectrometer put at the end of the beam line. A thin aluminum filter (thickness ≈ 200 nm) is used to block the remaining IR drive laser radiation, leaving only the high-harmonics beam. Then a transmission grating disperses the spectral components, which are recorded by a XUV camera (*Andor^{TM} DO420*).

The grating is made of 10.000 lines/mm (grating period of 100 nm with a slid width of 50 nm). It was fabricated at DIMES (Delft University of Technology, The Netherlands). The grating structure is etched in a 300 nm-thick silicon nitride (Si_3N_4) membrane which is deposited on a silicon wafer. After creating the transmission grating in the silicon nitride film over an area of 1 by 4 mm, the silicon at the backside of the film is remove using a wet etching method. This leaves a free-standing transmission grating. To improve

the resolution of the transmission grating, a 200 μm wide slide is placed in front of the grating.

A translation stage allows to position a simple hole instead of the grating, in order to directly measure the XUV beam profile with the XUV camera..

2.4 Recording of high-harmonic radiations

For the 150 μm diameter capillary filled with xenon gas, the typical drive laser pulse energy at the entrance of the capillary is typically around 0.6 mJ. The drive laser pulses energy is set by using the half-wave plate and the two polarizing beam splitters. Using these optics might induce an additional dispersion on the ultrashort pulse, effect which is investigate in Section 3.3. A shutter is also added in the beam path and remote-controlled by the software used to record the spectra. It allows to modify the exposure time and thereby to avoid saturation of the XUV camera.
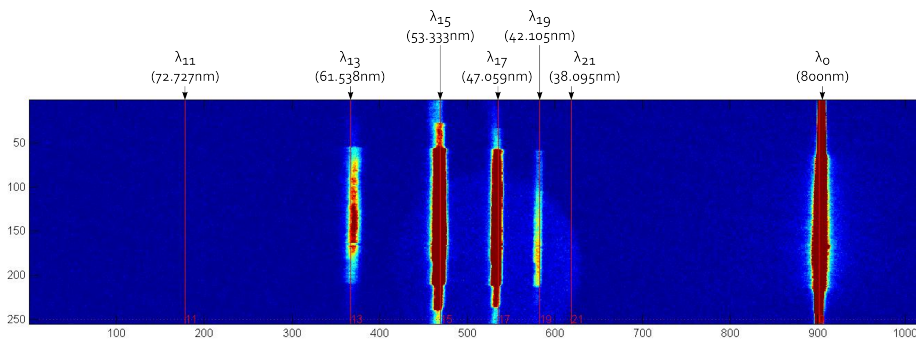
Figure 2.3: High-harmonic spectrum produces using xenon at a pressure of 35 mbar and an exposure time of 2 s. The brightest column to the right is the zeroth diffraction order, the others are the odd harmonic orders from 13 to 19.

The capillary is filled with xenon and high-harmonic can be generated. First the scintillator is used to check out if high-order harmonics are generated. Then, either the beam profile is measured by the XUV camera directly or the spectrum is measured by inserting the transmission grating in the XUV path.

To investigate pressure tuned phase matching in the capillary (see Section 1.2.1), we have varied the gas pressure and measured the relative intensity of the various harmonics. To improve measurement accuracy, the exposure time of the XUV camera was adjusted to maximum illumination of the CCD. A typical example of the measured spectrum is shown in Figure 2.3 for a pressure of 35 mbar and an exposure time of 2 s. The relative intensity of each order present in this spectrum is shown in the Figure 2.4. From these measurements the average maximum relative intensity per shot has been determined for each order as a function of pressure and is plotted in Figure 2.5. For our experimental conditions and for this harmonic, optimum phase-matching is reached for a pressure of approximately 33 mbar.
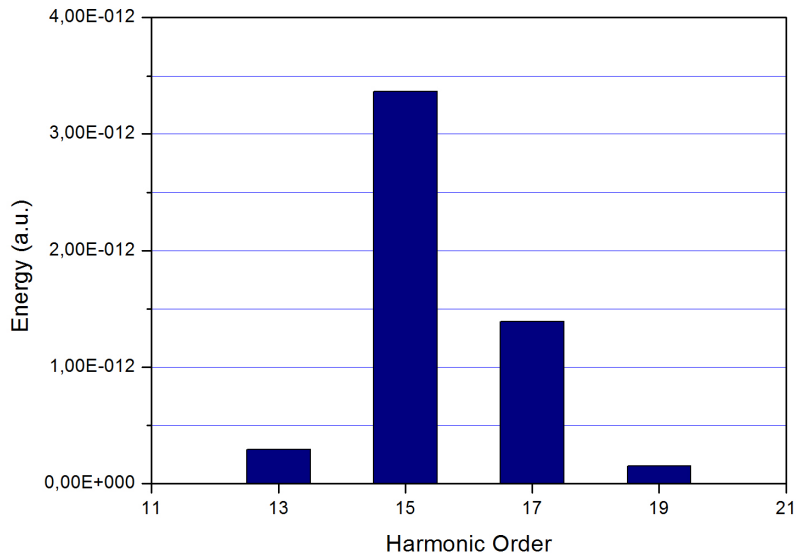
Figure 2.4: Relative energies of the harmonics produced in xenon at a pressure of 35 mbar and an exposure time of 2 s.
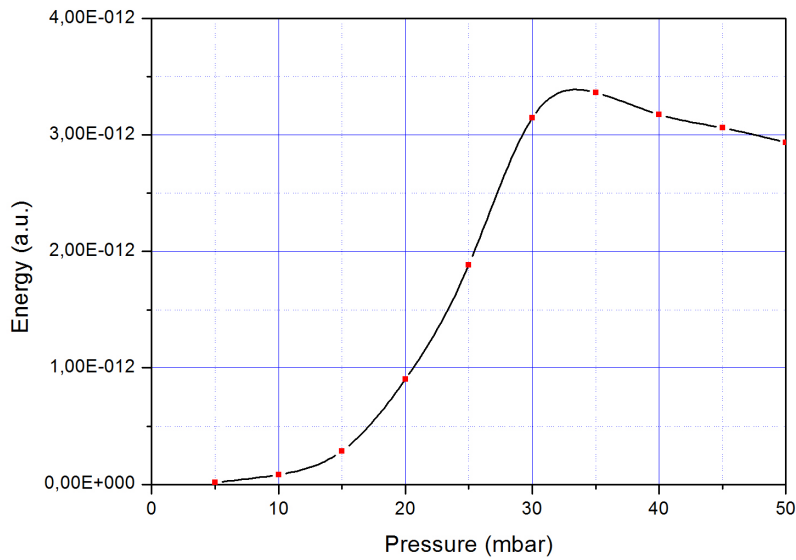

Figure 2.5: Relative energy of the 15th harmonic produced in xenon as a function of the pressure into the capillary.

Chapter 3

Tuning and selective enhancement

The ability to tune or selectively enhance a particular order of the high-harmonic spectrum can have significant advantages for applications. Indeed, high-harmonic generation only produces odd harmonics of the fundamental frequency. For instance, for the seeding of a free electron lasers, it could be necessary to tune these harmonics in order to fit one of them with the spectral gain area of the free electron laser. The enhancement is required to improve the seed power in the spectral gain area of the FEL, and thereby the quality of the seed.

Both selective enhancement and tuning of the harmonics can be obtained by shaping of the drive laser pulse. As mentioned in Chapter 1, the phase and spectrum produced by a single ionization-recombination event depends on the local drive laser field that first ionizes an atom and subsequently provides the kinetic energy available at recombination. Thus by shaping the drive laser pulse, we modify the local field within the drive laser pulse and can influence the phase and spectrum of the emission at recombination. Because of these changes, a particular harmonic can be enhanced and shifted in wavelength. The shaping of the drive laser pulse is done using a so-called acousto-optic programmable dispersive filter (AOPDF). The operating principle will be described in the first section of this chapter.

To understand how an AOPDF affects the drive laser pulse, a model of this device is created in Matlab™ and this model can be used to predict the pulse shape. This is important, as certain shaping may result in pulses that can damage the regenerative amplification stage in the Coherent™ amplifier. This model is described in the second section of this chapter. Finally, the last section reports about first experiments done with the AOPDF, where group delay dispersion was introduced and verified using GRENOUILLE.

3.1 Acousto-optic programmable dispersive filter

An acousto-optic programmable dispersive filter (AOPDF) is a device allowing for ultrashort pulse shaping in Chirp Pulse Amplification (CPA) and Optical Parametric Amplification (OPA) laser chains. Composed by a birefringent uniaxial crystal coupled to an piezoelectric transducer and a RF generator, it can be made from a number of crystals, such as $LiNbO_3$, $PbMoO_4$ or TeO_2 (the one used in the Dazzler™ device), and can be operated in a bulk wave design or in a surface wave design. It performs a convolution

between an input optical signal and a signal $S(t/\alpha)$ where $S(t)$ is the acoustic signal proportional to the electrical signal applied to the piezoelectric transducer of the device and α a scaling factor related to the ratio between the speed of sound and the speed of light in the material. The result of the convolution, the output signal, is contained in the diffracted output beam of the crystal.
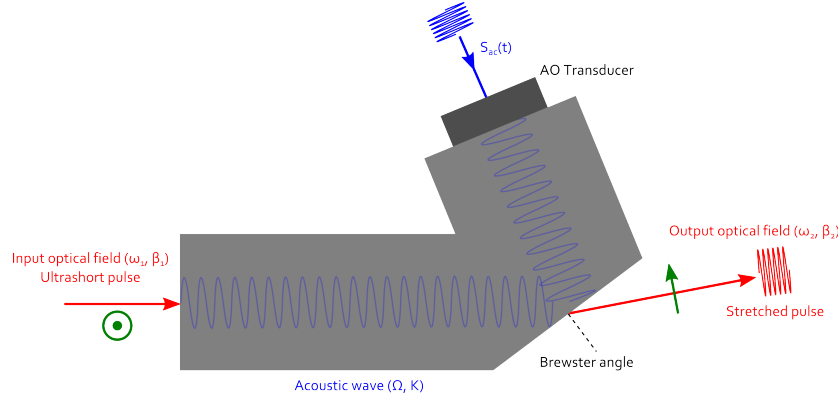

Figure 3.1: Collinear AOPDF device configuration.

AOPDF are commonly used for two kind of applications. The first kind of applications using the AOPDF concerns the corrections of group-delay dispersion introduced by the CPA laser chains, both in phase for the compensation of high-order phase distortions and in amplitude for the compensation of gain narrowing. These compensations are obtained simultaneously [12]. The second kind of applications of the AOPDF concerns the amplitude and phase shaping for coherent control of electronic or vibrational transitions in atomic, molecular and condensed matter physics [13].

3.1.1 Compensation of group delay time dispersion

Pierre Tournois was the first to demonstrate that using an acousto-optic interaction in an anisotropic birefringent medium it is possible to produce a chirped optical signal reproducing an original acoustic signal [12]. This acoustic signal can then be used to generate a pre-distorted optical signal at the input of a laser chain to compensate for group-delay dispersion within the chain.

This device makes use of the collinear and directional coupling between the ordinary and the extraordinary optical waves via an acoustic wave. The acoustic wave carries the programmable error signal that is transferred from the incident optical wave to the diffracted optical wave to compensate for the group delay time dispersion. The usual configuration of an AOPDF is shown in Figure 3.1 and the coupling between the optical waves and the acoustic wave is schematically shown in Figure 3.2.

The convolution process made by the AOPDF can be mathematically described as follows. Considering a collinear acousto-optic interaction in an anisotropic photoelastic medium, an incident optical wave $S_1(\omega_1, \beta_1)$ is coupled to a diffracted optical wave $S_2(\omega_2, \beta_2)$ through interaction with an acoustic wave $S_{ac}(\Omega, K)$. The nonlinear acousto-electric interaction results in a coupling between the waves:

$$S_1(\omega_1)e^{i(\omega_1 t - \beta_1 x)} \times S_{ac}(\Omega)e^{i(\Omega t - K x)} = S_2(\omega_2)e^{i(\omega_2 t - \beta_2 x)} \tag{3.1}$$

where $S_1(\omega_1)$, $S_{ac}(\Omega)$ and $S_2(\omega_2)$ stand respectively for the complex spectral amplitudes of the incident optical signal, the acoustic signal and the diffracted optical signal.

In the vicinity of the phase-matching conditions, $\omega_2 = \omega_1 + \Omega$ and $\beta_2 = \beta_1 + K$, the incident optical energy is transferred to the diffracted optical wave:

$$S_2(\omega_2) = S_1(\omega_1) \times S_{ac}(\Omega) \tag{3.2}$$

or, by taking the inverse Fourier transform to obtain the complex field amplitudes in the time domain,

$$s_2\left(t - \frac{n_2 x}{c}\right) = s_1\left(t - \frac{n_1 x}{c}\right) \otimes s_{ac}\left(t - \frac{x}{v}\right) \tag{3.3}$$

where $s_1(t)$, $s_{ac}(t)$ and $s_2(t)$ are respectively the complex amplitudes of the incident optical signal, the acoustic signal and the diffracted signal. n_1 and n_2 are the optical indexes of the photoelastic material for the incident and diffracted wave, v is the velocity of the acoustic wave and c is the velocity of light in vacuum. As a consequence, when the higher order terms of the nonlinear interaction are negligible in comparison to Equation 3.1, the diffracted optical signal is the convolution of the incident optical signal with the acoustic signal. $s_2(t)$ can then be considered as the result of the filtering of $s_1(t)$ by a programmable filter with impulse response $s_{ac}(t)$.
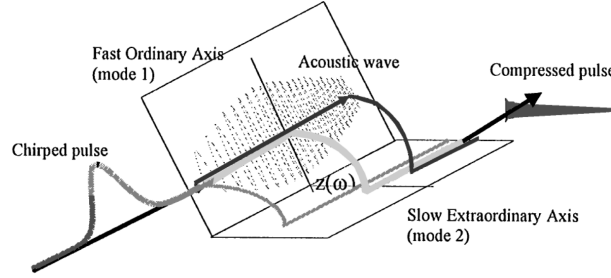
Figure 3.2: Schematic of the coupling of the optical waves by the acoustic wave in an AOPDF.

When the incident optical signal is a very short pulse and the acoustic signal is a long pulse with duration T_{ac} chirped inside a bandwidth B_{ac}, the diffracted optical signal is a long pulse with duration T_{opt} chirped inside a bandwidth B_{opt} and is the optical temporal image of the acoustic pulse. This regime can be named an acousto-optic programmable dispersive filter. Because of the conservation of information between acoustic and optical signals, $\frac{B_{ac}}{\Omega} = \frac{B_{opt}}{\omega_1}$ and $B_{ac}T_{ac} = B_{opt}T_{opt}$. Furthermore, taking the phase-matching conditions into account as:

$$n_2 \frac{\omega_2}{c} = n_2 \frac{\omega_1 + \Omega}{c} = n_1 \frac{\omega_1}{c} + \frac{\Omega}{v} \tag{3.4}$$

the optical and acoustic frequencies, bandwidths and pulse durations of an AO-PDF are given by:

$$\frac{\Omega}{\omega_1} = \frac{B_{ac}}{B_{opt}} = \frac{T_{opt}}{T_{ac}} = \frac{|n_2 - n_1|v}{c\left(1 - \frac{n_2 v}{c}\right)} \approx |n_2 - n_1|\frac{v}{c} \tag{3.5}$$

3.1.2 Amplitude and phase control of ultrashort pulses

An AOPDF device utilizing a perfectly collinear interaction for the optical and acoustic wave vectors allows for a larger group delay time dispersion compensation in CPA laser chains. First, the filter permits precompensation for gain narrowing, through amplitude shaping before amplification. Second, it allows phase errors that arise from imperfect matching of the dispersions of the pulse-lengthening elements and the compressor to be

corrected. A theoretical analysis of using amplitude and phase shaping of ultrashort pulses shows that a longitudinal AOPDF can manipulate both in amplitude and phase at the same time, femtosecond light pulses in the range of hundreds of THz by means of electrical signals in the range of a few tens of MHz [14, 13], in agreement with Equation 3.5. Some experiments using closed-loop amplification systems with the feedback of a FROG or a SPIDER have demonstrated optimization of the the output of a laser amplifier in a CPA setup [15]. However, the spectral amplitude pulse shaping may remain tricky because of the saturation and the damage threshold of the amplifier.
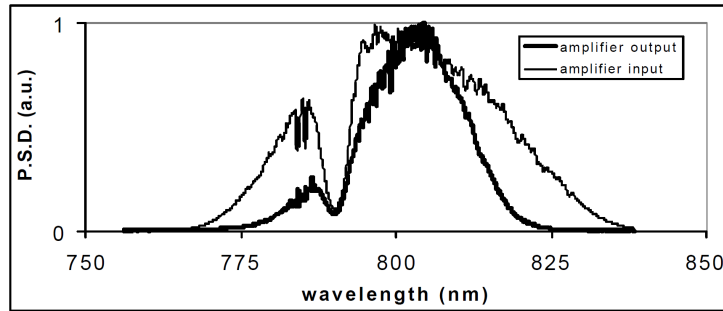
Figure 3.3: Spectral amplitude shaping in front of an amplifier. A hole was introduced at 790nm to avoid saturation of the amplifier. Adapted from [15].

The AOPDF is really a versatile device which allows for some freedom for shaping the pulses in the time and frequency domains. For instance, the incoming pulse can be split into several pulses that are separated in both the spectral and the temporal domains. The separation in time is achieved by application of different group delays to different spectral components, and the spectral separation is obtained by amplitude shaping [14].
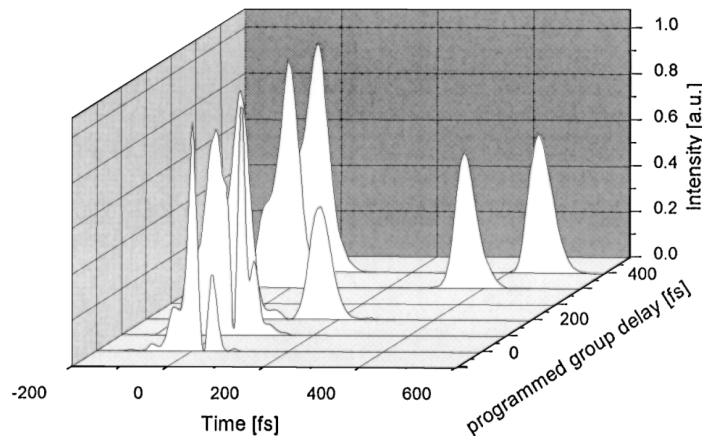
Figure 3.4: FROG measurement of the generation of two pulses separated by a programmable delay. Adapted from [14].

Pierre Tournois, with his society FastLite, developed the Dazzler™, a device based on an AOPDF especially designed for pulse shaping purposes in CPA setup. The Section 3.2 treats of the building of a numerical model of the pulse shaping by the Dazzler™ with Matlab.

3.2 Modeling of the Dazzler™ with Matlab™

The Dazzler™ is an AOPDF aimed for the pulse shaping of ultrashort light pulses in CPA chains of after an optical parametric amplification (OPA). This device consists of an AOPDF using a TeO_2 crystal, coupled to a RF generator driven by a computer provided with a software. The model used in our setup is the Dazzler™ HR-800/T1. The RF generator is the source of the analog high power RF signal but it also deals with the triggering process and other functions that can not be treated by the computer. The computer controls the settings and programming of the waveform, as well as storing or loading it from the hard disk. The time required to load a waveform (computing and transfer time to hardware memory) takes approximately 850ms. Therefore, the waveform can be updated with a repetition rate of maximum 1 Hz.

Its numerical modeling by Matlab™ is firstly motivated by the protection of the amplifier. Indeed, because of the saturation and the damage threshold of the amplifier, it is necessary to check for the creation by the Dazzler™ of unexpected shapes. For instance, it is necessary to avoid creation of isolated high power peaks in the amplitude spectrum, or spectral narrowing which makes the pulse much shorter and the energy added to the pulse by the regenerative amplifier is then in pulse of shorter duration. Hence, the power increases and can become larger than the damage threshold of the regenerative amplifier. The second reason which motivates the numerical modeling is because it is a simple and effective way to get an idea of the pulse shaping capabilities of the Dazzler™.
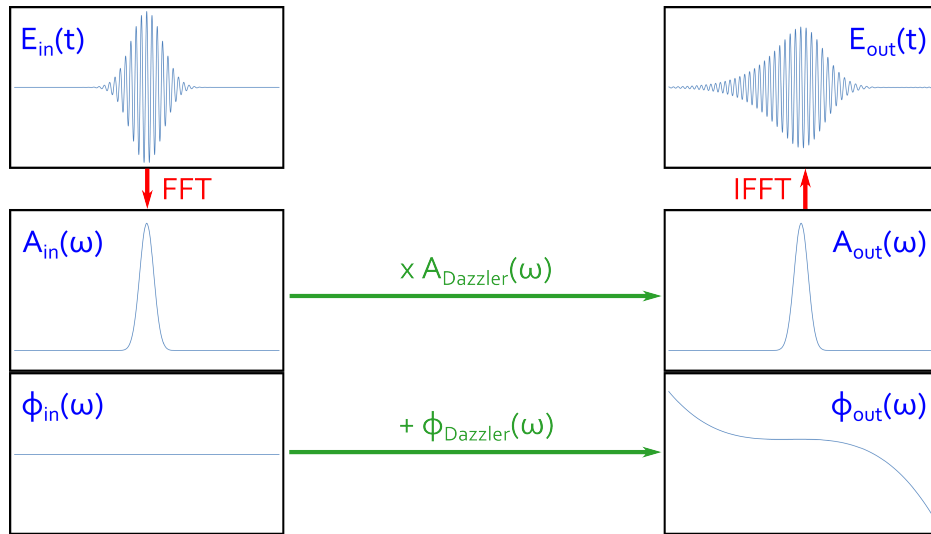
Figure 3.5: Logical schema summarizing the main steps of the algorithm.

The process of this model, summarized in Figure 3.5, is the following: first, from the given parameters, the software generates an unchirped Gaussian or $Sech^2$ pulse in the form of a matrix. The matrix is used to store both the temporal coordinate (first row) and the normalized electric field (second row). The generation of this input pulse is based on the following formulas:

$$E_{Gaussian}(t) = e^{2\ln 2\left(\frac{t}{\tau_p}\right)^2} \times e^{j\omega_0 t} \tag{3.6}$$

$$E_{Sech^2}(t) = sech\left(\frac{t}{\tau}\right) \times e^{j\omega_0 t} \tag{3.7}$$

where $\omega_0 = 2\pi\nu_0$ and $\tau \approx 1.76 \times \tau_p$, with ν_0 the central frequency of the pulse and τ_p the pulse width defined in the usual FWHM fashion [16].

The spectral amplitude and spectral phase of the input pulse are then "extracted" from the matrix using the Fast Fourier Transform (FFT) algorithm of Matlab™. The input spectral amplitude $A_{in}(\omega)$ is defined as the absolute value (abs) of the FFT of the input electric field $E_{in}(t)$. The input spectral phase $\phi_{in}(\omega)$ is defined as the phase angle (angle) of the FFT of the input electric field $E_{in}(t)$. Both are stored into respective matrices.

Now that the input pulse is defined, we have to implement the action of the Dazzler. As this device can both shape the amplitude and phase of the optical pulse, the action of the Dazzler is applied to the signal in the frequency domain via two transfer functions, one for the phase (additive) and one for the amplitude (multiplicative), as is shown in figure 3.5. The amplitude transfer function can be quite general, and we illustrate here a particular example that results in the creation a hole in the spectrum at a particular wavelength. This hole is define by its position λ_1 (nm), its width $\delta\lambda_1$ (nm) and its depth k ($0 \leq k \leq 1$). The phase transfer function allows to add a delay, a broadening or/and a chirping in the input spectral phase. The parameters used for it are the first order a_1 (linear phase), the second order a_2 (second order polynomial phase), the third order a_3 (third order polynomial phase) and the fourth order a_4 (fourth order polynomial phase). They correspond to the first four orders in the power series expansion of the phase transfer function and can each be used independently of the others

The amplitude and phase shaping functions of the Dazzler, also stored in the form of matrices, are calculated from the provided parameters using:

$$A_{Dazzler}(\omega) = 1 - k.e^{-\left(\frac{\omega - \omega_1}{\delta\omega_1}\right)^2} \tag{3.8}$$

$$\phi_{Dazzler}(\omega) = -\left(a_1(\omega - \omega_0) + \frac{a_2}{2}(\omega - \omega_0)^2 + \frac{a_3}{6}(\omega - \omega_0)^3 + \frac{a_4}{24}(\omega - \omega_0)^4\right) \tag{3.9}$$

with $\omega_1 = \frac{2\pi c}{\lambda_1}$, $\chi_1 = \frac{\delta\lambda_1}{2\lambda_1}$ and $\delta\omega_1 = \omega_1.\frac{(\chi_1 - \chi_1^3)}{2}$ [17].

The output spectral amplitude $A_{out}(\omega)$ is then obtained by multiplying the input spectral amplitude with the amplitude transfer function of the Dazzler, and the output spectral phase $\phi_{out}(\omega)$ by adding the input spectral phase with the phase transfer function of the Dazzler:

$$A_{out}(\omega) = A_{in}(\omega) \times A_{Dazzler}(\omega) \tag{3.10}$$

$$\phi_{out}(\omega) = \phi_{in}(\omega) + \phi_{Dazzler}(\omega) \tag{3.11}$$

With the output amplitude and phase spectra, it is now possible to retrieve the shape of the output pulse. The electric field of the output pulse in time domain is provide by the Inverse Fast Fourier Transform (IFFT) of its expression in the frequency domain, obtained with this formula:

$$E_{out}(\omega) = A_{out}(\omega).e^{-i.\phi_{out}(\omega)} \tag{3.12}$$

Stored into an other and last matrix, this output pulse can finally be plotted and compared to the input pulse.

A user manual for this model can be found in Appendix B, whereas the source code is available in Appendix C.

A future enhancement for this model could be to have the possibility to load all kind of pulse shapes from miscellaneous sources, the current version being limited to the creation

of perfect unchirped Gaussian or Sech^2 pulses.

3.3 Zero-dispersion settings

When a light pulse propagates through a transparent medium, it experiences group delay dispersion [18]. The crystal of the Dazzler, as well as the optics such as half-wave plate and the vacuum window, don't make exceptions. The original pulse width at the output of the amplifier is then broadened all along the setup before it reaches the capillary.

The Dazzler software possesses a self-compensation function, which allows for loading a waveform that compensates the dispersion induced by the crystal. When used, the second, third and fourth orders controls are set to the opposite of the corresponding values for the dispersion of the crystal in ordinary polarization mode. Hence, with this setting, the Dazzler device is dispersion free. For the Dazzler used in our experiment, the self-compensation waveform is set with the following phase settings:

$$a_2 = -12845 \text{ fs}^2, \, a_3 = -7396 \text{ fs}^3 \text{ and } a_4 = -2611 \text{ fs}^4. \tag{3.13}$$

Note, first order phase only affects the delay through the crystal and is therefore not important for self-compensation. The maximum delay that can be applied is however limited by the length of the crystal. However, even with the compensation of the dispersion induced by the crystal of the Dazzler, it is still necessary to compensate for the dispersion induced by the other transparent optics used in our setup, in order to set the pulse width in the capillary as short as possible. As seen in Section 3.1.1, the Dazzler can be used in that purpose, by modifying the phase parameters of the loaded waveform.
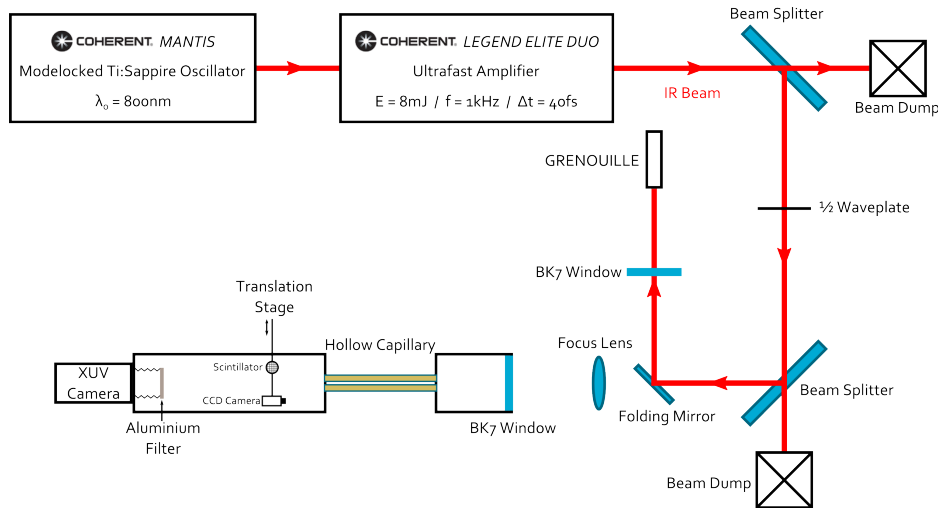
Figure 3.6: Simple sketch of our setup for for GRENOUILLE measurements.

The pulse width is measured with the GRENOUILLE at a distance after the amplifier corresponding to the position of the capillary. The ultrashort pulse experiences the same beam path as for the generation of high-harmonics, except for the focus lens which can not be used with the GRENOUILLE, because of the presence of other lenses in the GRENOUILLE setup. A folding mirror is positioned in front of the focus lens and send the beam through an other window, which is the same as the vacuum window, and into the GRENOUILLE. The results are compiled into a graphic shown in Figure 3.7.

A first observation is that the shortest possible pulse width is not obtained with the zero-dispersion setting of the Dazzler™ for the second order, -12845 fs^2, but for the
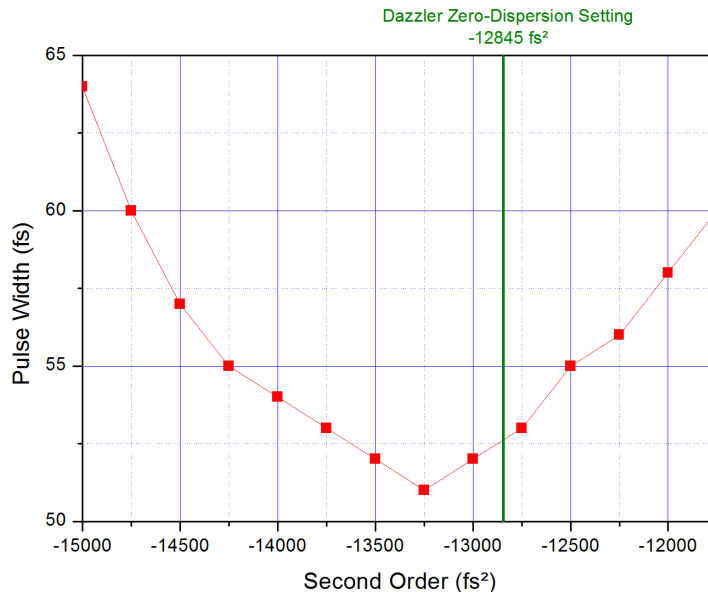
Figure 3.7: GRENOUILLE measurements of the pulse width as a function of the second order phase setting of the Dazzler™. The other phase settings are fixed.

value -13250 fs^2. This makes sense because of the dispersion induced by the optics (half-wave plate, vacuum window), the difference in the second order setting being the needed correction to compensate this dispersion.

Second observation, taking into account the limited resolution of the GRENOUILLE ($\approx 1 fs$, with some fluctuations on the lower decimals), the initial pulse width measured just at the output of the amplifier ($\tau_{GR} \approx 50$, see Section 2.1) could not be reached again by playing only with the second order setting of the Dazzler™. The GRENOUILLE setup contains lenses, a prism and a nonlinear crystal, that is transmission optics. Hence the measurement device induces group-delay dispersion as well, that will result in a broadening of the pulse. This may explain the 1 fs difference. However, the same study of the evolution of the pulse width by modifying the third or the fourth order in the neighborhood of the zero-dispersion setting of the Dazzler™ did not reveal any relevant or measurable effect with our setup.

From these results, we can assume that the shortest pulse width that is possible to get in the capillary is obtained for the following phase configuration of the waveform loaded by the Dazzler™:

$$a_2 = -13250 \text{ fs}^2, a_3 = -7396 \text{ fs}^3 \text{ and } a_4 = -2611 \text{ fs}^4. \tag{3.14}$$

However, this assumption is made while the focus lens is not include in these measurements and taking into account the group-delay dispersion of the GRENOUILLE, which is not present in the actual beam path to the capillary.

3.4 Qualitative studies of the effect of pulse shaping on the high-harmonic spectrum

The previous study gave an overview of how the pulse width is affected by the phase settings of the Dazzler™. The next step focuses on the main interest of this work, the

behavior of the high-harmonic generation while modifying the waveform of the drive laser pulses. Each phase order setting is used separately and independently of the other. The high-harmonic spectrum is recorded for several values of the second order phase setting, then for several values of the third order. The energy of the 13th, 15th, 17th and 19th harmonics are extracted from each of these spectra.

3.4.1 Second order

The high-harmonic spectrum is recorded for values of the second order phase setting from -15000 fs^2 to -10500 fs^2, with a step of 100 fs^2, while third order phase is set to -7396 fs^3 and fourth order phase is set to -2611 fs^4. A graphic shown in Figure 3.8 shows the evolution of the energy of each harmonic as a function of the second order phase setting.
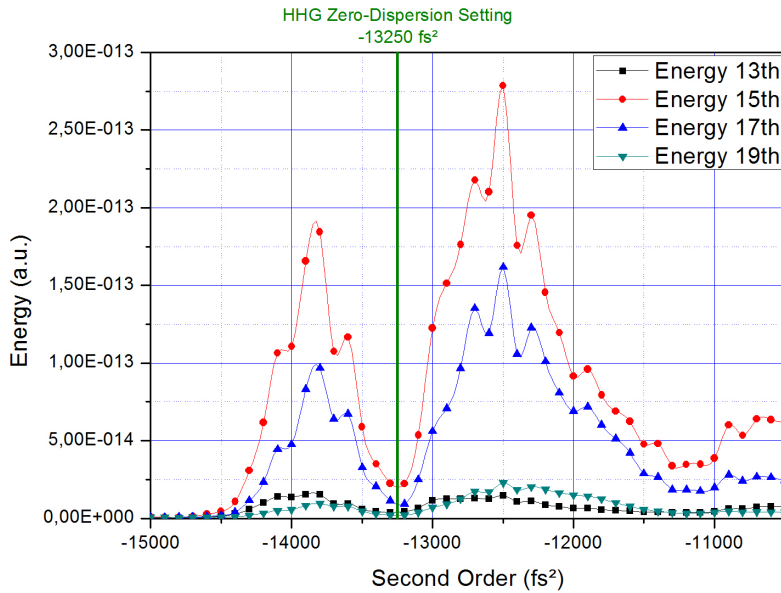
Figure 3.8: Relative energy of the harmonics as a function of the second order phase setting of the Dazzler™.

First observation, the maximum energy for each of the harmonics is not obtained for the zero-dispersion setting established in the previous Section (-13250 fs^2), but for the second order phase setting value -12500 fs^2. Further we observe that all the harmonic reach local maxima and minima at the same value for the second order phase. Moreover, the zero-dispersion setting provides a minimum of energy in the harmonics. As the value of the second order phase of -12500 fs^2 is even smaller that the value of -12850 fs^2 used for self-compensation of the Dazzler, we conclude that the high harmonics generation is maximum when the pulse in the capillary has not the shortest duration. In comparison with the zero-setting configuration of the Dazzler, we have here about a 50 % increase in yield. Referring to Figure 3.7 we conclude that a pulse width close to 55 fs leads to the highest yield of high harmonics.

Second observation, there is a secondary energy peak, whose the energy ratio to the main energy peak is not the same for each harmonic order. The ratio between the maximum of the secondary peak and the maximum of the main peak, E_{Second}/E_{Main}, for each harmonics is shown in the Table 3.1.

However, for the 13th order, the secondary energy peak is lightly higher than the main

Table 3.1: Ratio between the secondary energy peak and the main energy peak for each harmonics.

Harmonic Orders	13th	15th	17th	19th
Energy Peaks Ratio	105.7%	66.2%	59.8%	40.8%

energy peak. This last result is nevertheless to be considered with precaution, because of the weak signal registered for the 13th order.

From the spectra, it is also possible to analyze the spectral width and the wavelength of the harmonics. For the spectral widths, no significant change for any of the harmonic order is observed. For the wavelengths, a shift can be observed for all the harmonics, as shown in Figure 3.9. However, the shift is associated with a drop in energy of the harmonic. It is also noticeable that the shift occurs in the same direction, no matter if the second order phase setting is increased or decreased.
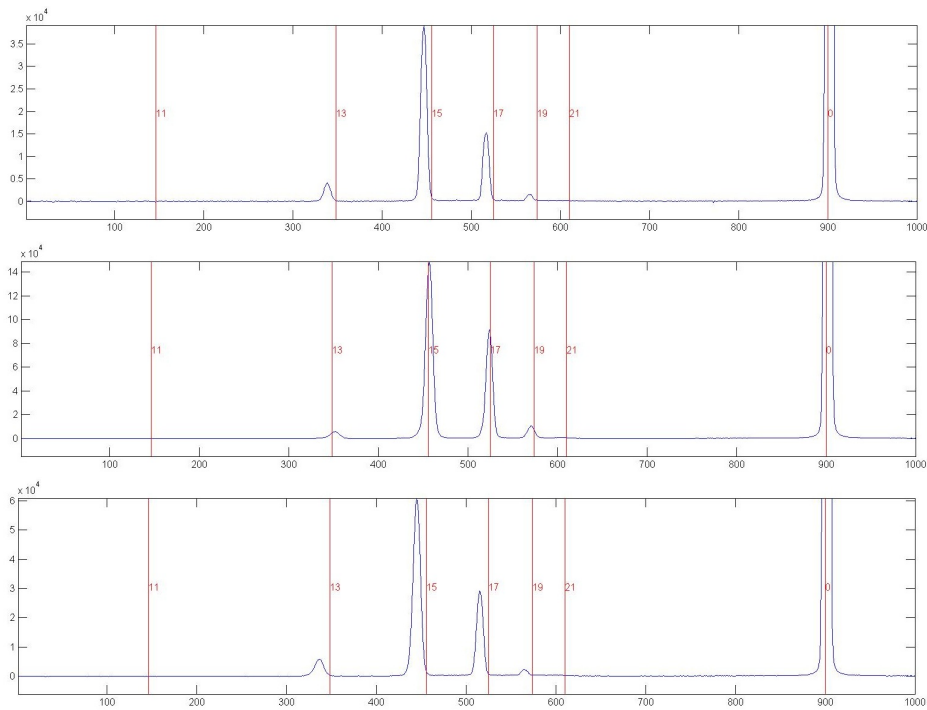
Figure 3.9: High-harmonic spectrum (xenon, pressure of 35 mbar, exposure time of 2 s) recorded for three different values of the second order phase setting of the Dazzler™: (a) -10500 fs^2, (b) -12500 fs^2 and (c) -14000 fs^2.

3.4.2 Third order

The high-harmonic spectrum is recorded for values of the third order phase setting from -35000 fs^3 to -5000 fs^3, with a step of 1000 fs^3 while second order phase is set to -13250 fs^2 and fourth order phase is set to -2611 fs^4. A graphic shown in Figure 3.10 shows the evolution of the energy of each harmonic as a function of the third order phase setting.

The response of the HHG process to the third order phase variation is less pronounced than that to the second order phase. The yield seems to remain constant within 15 % over a broad range of values before it starts to decrease for settings below -20000 fs^3.

From the spectra, it is also possible to analyze the spectral width and the wavelength of the harmonics. However, no significant change is observed, neither for the spectral
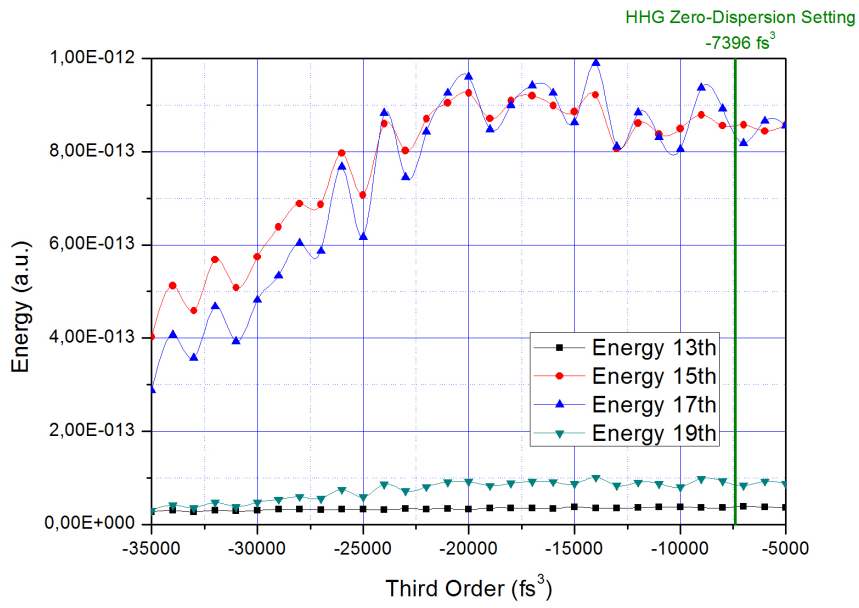
Figure 3.10: Relative energy of the harmonics as a function of the third order phase setting of the Dazzler™

widths, nor for the wavelengths.

Summary

This work allowed first to confirm and validate the previous experiments by producing successfully high-harmonic radiations with xenon. The spectrum of the generated harmonic radiation was successfully measured and, so far, we were able to generate radiation with a cut-off wavelength of 42 nm (30 eV), corresponding to the 19th harmonic of the 800 nm wavelength of the drive laser. The tuning of the phase-matching conditions by the gas pressure has also been demonstrated again experimentally. It is planned to use a different capillary with a larger diameter, in order to increase the interaction volume and maybe to improve the high-harmonic output.

A first numerical model of the Dazzler™ was made and used to get a first global idea of which kind of shaping is possible with this device. The model could yet be improved, for instance by adding the possibily to use as input any kind of pulses, calculated or recorded by an other device.

We also presented the first experiments of high-harmonic generation done with pulse shaping of the drive laser field by using of the Dazzler™. The results obtained from these experiments are really encouraging since they show an influence of the pulse shaping by the Dazzler on the high-harmonic output. More specifically, one of the desired effect, the tuning, was demonstrated using the second order phase setting, although the yield was reduced.

Still the results are promising. So far only one parameter has been varied at the time and to tune and selectively enhance a particular harmonic requires optimization in a multi-dimensional parameter space. Such kind of optimization is ideally the playground of evolutionary algorithms. Such a control algorithm will be implemented in the near future and these initial measurement, together with other planned measurements, will help us to understand the individual effect of each of the parameters used in the optimization process.

Appendix A

Ultrashort pulse measurements

A.1 Interferometric autocorrelation

Intensity autocorrelation is a method of measurement for ultrashort pulses, using the cross-correlation of a pulse with itself. This method was developed because it was realized that no shorter event existed with which to measure an ultrashort pulse.

In an intensity autocorrelator as shown in Figure A.1, a beam splitter splits an incoming pulse into two pulses, which are then focused and sent into a nonlinear-optical medium, such as a second-harmonic-generation (SHG) crystal. The arm length difference and thus the relative timing of the pulses can be mechanically adjusted via the variable delay line. If the arm length difference is made small, so that the pulses meet in the nonlinear crystal, the process of sum frequency generation occurs, leading to an output with a shorter wavelength. If the relative time delay is increased, so that the overlap of the two pulses in the crystal is reduced, the mixing product becomes weaker.
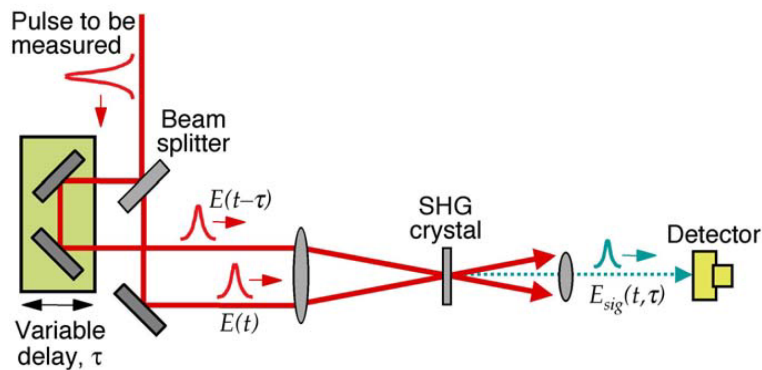
Figure A.1: Experimental layout for an intensity autocorrelator using second-harmonic generation.

For measuring the pulse duration, the power of the mixing product is recorded as a function of the arm length difference. The dependence of the autocorrelation signal on the temporal delay is given by

$$A(\tau) = \int_{-\infty}^{+\infty} |E(t)E(t - \tau)|^2 \, dt = \int_{-\infty}^{+\infty} I(t)I(t - \tau) dt \qquad (A.1)$$

with $I(t) = |E(t)|^2$. $A(\tau)$ is called the intensity autocorrelation.

For our experiments, a *Femtochrome FR-103XL*, a high-resolution autocorrelator, is used. This instrument is aimed for continuous monitoring and display of femtosecond and picosecond laser pulses from modelocked lasers with high peak power. The Figure A.2 shows the autocorrelator trace, with a width $T = 3.75$ μs, obtained from the ultrashort pulses at the output of the amplifier. This measurement needs to be calibrated in order to get the proper FWHM autocorrelation trace.
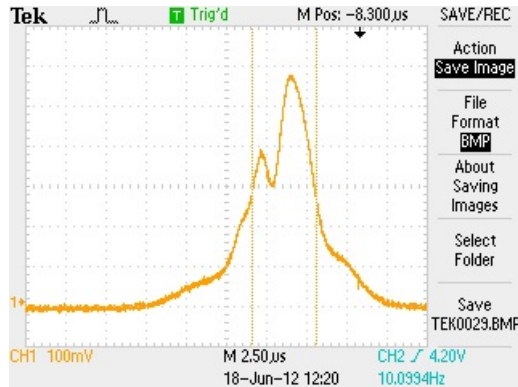
Figure A.2: Autocorrelator trace of the ultrashort pulses at the output of the amplifier.

The calibration factor can be determined by translation of the micrometer driven retroreflector stage in the stationnary arm of the autocorrelator. For a given translation x, the corresponding shift s in the position of the trace peak on the oscilloscope yields the calibration factor using the conversion formula:

$$\frac{t}{T} = \frac{2x}{0.3s} \ (\text{fs}/\mu\text{s}) \tag{A.2}$$

where x is in mm and s is in ms. For our experiment, for a translation $x = 0.1$ mm, the trace peak is shifted by $s = 0.035$ ms, providing a calibration factor $t/T = 19.05$ fs/μs. It is then possible to calculate the FWHM autocorrelation trace t:

$$t = 19.05 \times T = 19.05 \times 3.75 = 71.44 \ \text{fs} \tag{A.3}$$

The conversion from the FWHM autocorrelation trace width T to the FWHM pulse width τ is a function of the assumed pulse shape. For a sech^2 pulse shape, like in our experiment, the conversion factor is 0.648 (for comparison, it is of 0.707 for a gaussian pulse). Therefore, the pulse width τ measured with the autocorrelator is:

$$\tau = t \times 0.648 = 71.44 \times 0.648 = 46.29 \ \text{fs} \tag{A.4}$$

A.2 Grating-eliminated no-nonsense observation of ultrafast incident laser light e-fields (GRENOUILLE)

GRENOUILLE is an ultrashort pulse measurement technique based on FROG (*frequency-resolved optical gating*).

FROG is a technique for measuring ultrashort laser pulses, replacing autocorrelation, which only gave a rough estimate for the pulse length. FROG is simply a spectrally resolved autocorrelation, sharing the idea of combining a pulse with itself in a nonlinear medium. But where autocorrelators only measure the intensity of the nonlinear signal

and retrieve a pulse length from it, FROG also measures the spectrum of the signal at each delay. This measurement creates a spectrogram of the pulse, which allows the use of a phase-retrieval algorithm to retrieve the precise pulse intensity and phase vs. time. It can measure both very simple and very complex ultrashort laser pulses.
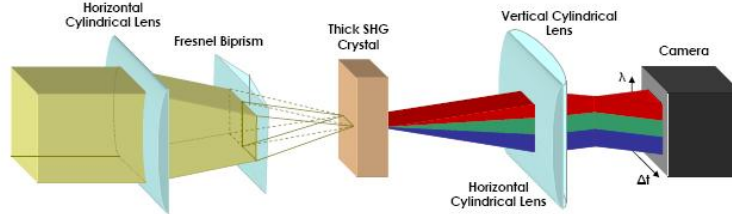
Figure A.3: Configuration of a GRENOUILLE. The light beams propagate from the left to the right.

Because most FROG techniques have an autocorrelator, they also have the sensitive alignment issues that come with it. In addition, most FROGs use a thin second harmonic generation (SHG) crystal and a spectrometer, adding signal strength requirements as well as additional alignment issues. GRENOUILLE is a simple device based on the SHG FROG. It replaces the beam splitter, delay line and beam recombination components of the autocorrelator with a prism while the spectrometer and thin SHG crystal combination is replaced by a thick SHG crystal (see Figure A.3). The effect of these replacements is to eliminate all sensitive alignment parameters while at the same time increasing the signal strength. These changes also reduce the complexity and cost of this type of system. Like the previous FROG systems however, GRENOUILLE still determines the full phase and intensity data of a pulse. GRENOUILLE produces traces identical in form to those from SHG FROG.

For our experiments, a homemade GRENOUILLE is used. A picture of it and its specifications are shown in the Figure A.4. The Fresnel biprism, which has a top angle $\alpha = 128°$, is placed in the focus of the first cylindrical lens. The BBO crystal, from the fabricant EKSPLA, is of type 1, with $\theta = 29.2°$ and $\phi = 90°$. Furthermore, it has an anti-reflection coating at 800nm and 400nm [19].

The FROG signal is read and analyzed by a software program called Video FROG, created by MesaPhotonics. This program is able to retrieve the complete pulse profile, with both the pulse duration and the spectral bandwidth. An example of measurement made with this software of the ultrashort pulses from the amplifier is shown in the Figure A.5.
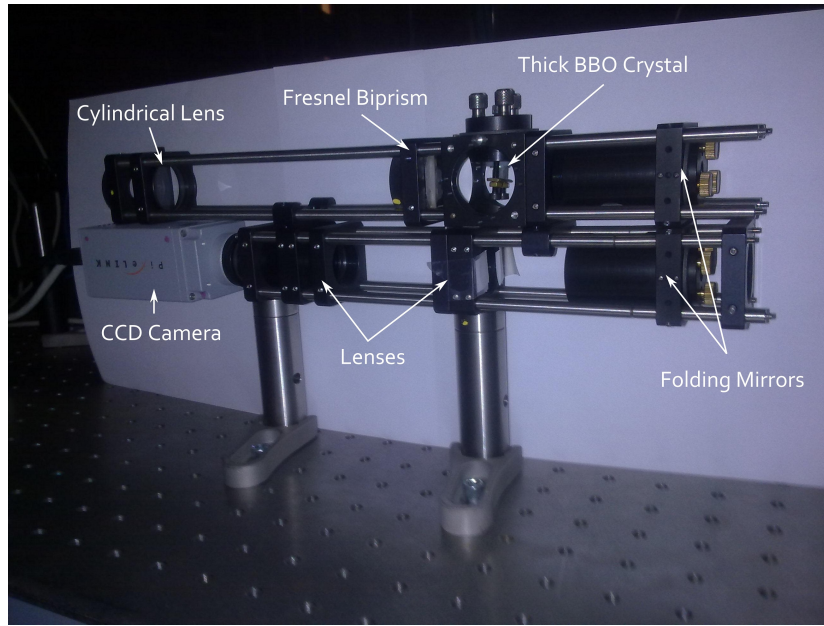
Description	Details
Cylindrical Lens	f = 208mm
Fresnel Biprism	$\alpha = 128°$
BBO Crystal	$5 \times 5 \times 5$
Lens	f = 208mm
Lens	f = 104mm
CCD Camera	PixeLINK

Figure A.4: Picture and specifications of our homemade GRENOUILLE.
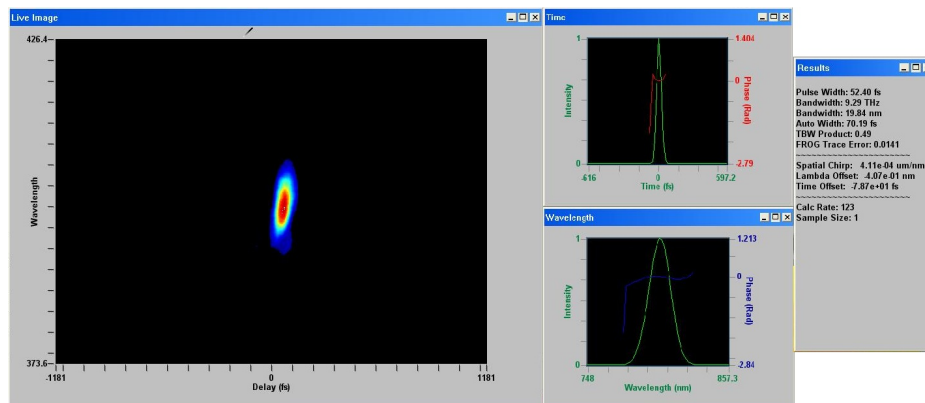
Figure A.5: GRENOUILLE measurement of the ultrashort pulses from the amplifier made with the Video FROG software. The beam profile is shown on the main window, with the time on the X-axis and the wavelength on the Y-axis. The two little windows depict a cut along the time axis and the wavelength axis, respectively. Intensity and phase are both represented. Finally, the last window provides results such as the pulse width, the bandwidth or the spatial chirp.

Appendix B

Dazzler™ modeling with Matlab™ - Manual

The software is composed of two Matlab™ files: MainPanel.m, which built the user's interface, and PulseCalculation.m, which implements the mathematical calculations. In order to run the software, use the file MainPanel.m. The user interface is divided into several areas, each identified by a different color, and associated with the main modeling blocks to simulate Dazzler performance. In the green area, the user supplies the input parameters and the input pulse is displayed both in the temporal and frequency domain. In the orange area, the users sets the action of the Dazzler by specifying parameters for the various orders of the phase and for amplitude transfer function that creates a hole in the spectrum. The gold area displays the shaped pulse, again in both the temporal and frequency domain. These areas will be discussed in more detail in the following sections.
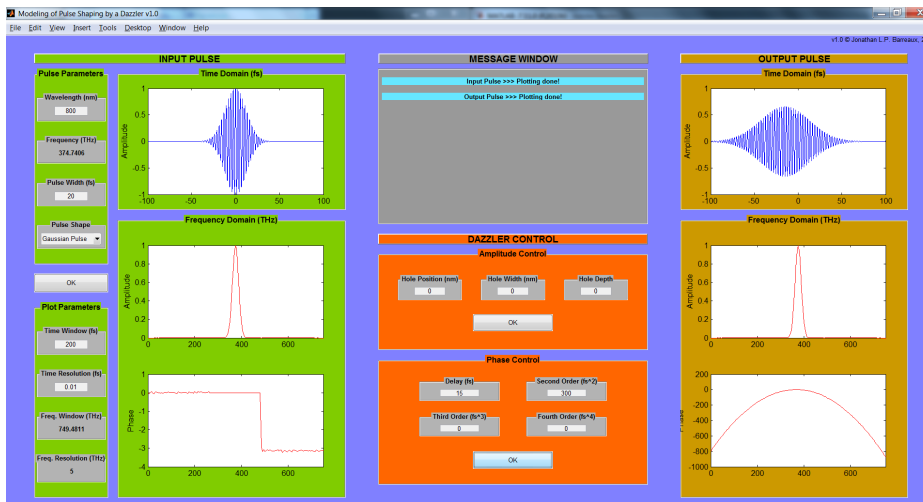
Figure B.1: Global view of the graphic interface.

B.1 Input Pulse

This green area allows you to set input parameters for the input pulse in time domain and its amplitude and phase (i.e. complex spectrum) in the frequency (Fourier) domain. The current version only allows to implement unchirped Gaussian or $Sech^2$ pulses.
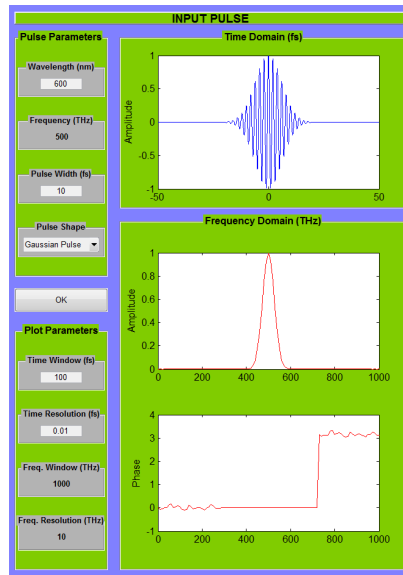
Figure B.2: Input Pulse area.

B.1.1 Pulse Parameters

This panel allows you to provide the parameters used to calculate the input pulse as a function of time:

- **Wavelength** λ_0 - *The central wavelength of the input pulse (in nm)*

- **Frequency** ν_0 - *The central frequency of the input pulse (in THz)*

  It is calculated from the central wavelength λ_0: $\nu_0 = \frac{c}{\lambda_0}$, where $c = 299792458$ m.s^{-1} is the velocity of light in vacuum.

- **Pulse Width** τ_p - *The width of the input pulse (in fs)*

  The pulse width is measured as full-width at half maximum (FWHM). Note that this is the FWHM pulse width for the intensity and not for the field [16].

- **Pulse Shape** - *The shape of the input pulse*

  Currently implemented choices are Gaussian and Sech^2 pulses.

See Section B.1.3 for the formulas used to calculate the electric field of the input pulse as a function of time $E(t)$ from these parameters.

B.1.2 Plot Parameters

This panel allows you to adjust the plotting parameters:

- **Time Window** t_{max} - *The size of the time domain window (in fs)*

  The input and output pulses are plotted from $\frac{-t_{max}}{2}$ to $\frac{t_{max}}{2}$. Artifacts could occur if the time window is not broad enough, due to the superimposition of data. Make always sure that the temporal pulse fits entirely in the time windows.

- **Time Resolution** t_{res} - *The plotting resolution of the time domain (in fs)*

  It defines the number of points used to make the plots of the input and output pulses in time domain. The time vector is generated from $\frac{-t_{max}}{2}$ to $\frac{t_{max}}{2}$ with a point every t_{res}.

- **Frequency Window** ν_{max} - *The size of the frequency domain window (in THz)*

  The spectral amplitude and spectral phase for the input and output pulses are plotted from 0 to $\nu_{max} = 2\nu_0$, where ν_0 is the central frequency of the input pulse.

  Note that this is a truncation of the real frequency window used by the calculations, which is set by the time resolution: $\nu'_{max} = \frac{1}{t_{res}}$.

- **Frequency Resolution** ν_{res} - *The plotting resolution of the frequency domain (in THz)*

  It is calculated from the time window: $\nu_{res} = \frac{1}{t_{max}}$; and defines the number of points used to make the plots of the spectral amplitude and spectral phase for the input and output pulses. The frequency vector is generated from 0 to $\nu_{max} = 2\nu_0$ with a point every ν_{res}.

B.1.3 Time Domain (fs)

This panel provides a graphic view of the electric field of the input pulse in the time domain. It is calculated from the input pulse parameters using one of the following formulas:

$$E_{Gaussian}(t) = e^{2 \ln 2 \left(\frac{t}{\tau_p}\right)^2} \times e^{j\omega_0 t} \tag{B.1}$$

$$E_{Sech^2}(t) = \text{sech}\left(\frac{t}{\tau}\right) \times e^{j\omega_0 t} \tag{B.2}$$

with $\omega_0 = 2\pi\nu_0$ and $\tau \approx 1.76 \times \tau_p$ [16].

For the rest of this document, the input electric field will be referenced as $E_{in}(t)$.

B.1.4 Frequency Domain (THz)

This panel provides a graphic view of the spectral amplitude and spectral phase for the input pulse. These are obtained by using the Fast Fourier Transform (FFT) algorithm of Matlab™, and the abs and angle functions. The input spectral amplitude $A_{in}(\omega)$ is defined as the absolute value (abs) of the FFT of the input electric field $E_{in}(t)$. The input spectral phase $\phi_{in}(\omega)$ is defined as the phase angle (angle) of the FFT of the input electric field $E_{in}(t)$.

B.2 Message Window

This gray area provides messages indicating if the plotting processes are done and/or if errors occurred. The colors of the error messages are linked with the concerning area/panel. General messages are in cyan.
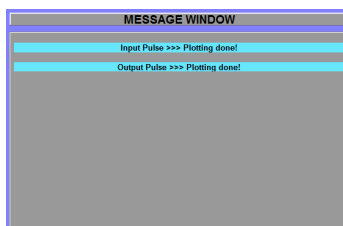
Figure B.3: Message Window area.

B.3 Dazzler Control

This orange area offers the same controls as offered by the control panel of the Dazzler user interface. The purpose of this model is to simulate the action of the Dazzler and calculated the shaped output pulse. To this end, the complex input spectrum is modified according to the settings in this control panel and via an inverse Fourier transform, the shaped output pulse is calculated in the time domain. By default, all the values are zero, and the input and output spectra are the same.
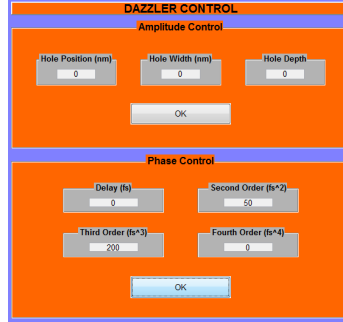
Figure B.4: Dazzler Control area.

B.3.1 Amplitude Control

The amplitude control allows to create a hole in the input spectral amplitude. Three parameters are necessary to completely specify the hole characteristics:

- **Hole Position** λ_1 - *The position of the hole in the spectrum (in nm)*

- **Hole Width** $\delta\lambda_1$ - *The width of the hole (in nm)*

- **Hole Depth** k - *The depth of the hole*

  It must be a value between 0 and 1 ($0 \leq k \leq 1$), the value 0 meaning no hole and the value 1 meaning a complete extinction of the specified wavelength.

These parameters must be all non-zero in order to create a hole. If at least one of these is zero, the amplitude shaping is ignored.

The amplitude transfer function of the Dazzler is modeled by the following formula:

$$A_{Dazzler}(\omega) = 1 - k.e^{-\left(\frac{\omega - \omega_1}{\delta\omega_1}\right)^2} \tag{B.3}$$

with $\omega_1 = \frac{2\pi c}{\lambda_1}$, $\chi_1 = \frac{\delta\lambda_1}{2\lambda_1}$ and $\delta\omega_1 = \omega_1.\frac{(\chi_1 - \chi_1^3)}{2}$ [17].

The output amplitude $A_{out}(\omega)$ is then obtained by multiplying the Dazzler induced amplitude with the amplitude of the input pulse:

$$A_{out}(\omega) = A_{in}(\omega) \times A_{Dazzler}(\omega) \tag{B.4}$$

B.3.2 Phase Control

The phase control allows to add a delay, a broadening and/or a chirping in the input spectral phase. The four parameters correspond to the first four orders in the power series expansion of the phase transfer function and can each be used independently of the others:

- **Delay** a_1 - *First order in the power series expansion (in fs)*

  Create a linear phase, resulting in a delay of the pulse in the time domain.

- **Second Order** a_2 - *Second order in the power series expansion (in fs^2)*

  Create a second order polynomial phase, resulting in a broadening of the pulse in the time domain.

- **Third Order** a_3 - *Third order in the power series expansion (in fs^3)*

  Create a third order polynomial phase, resulting in a chirping of the pulse in the time domain.

- **Fourth Order** a_4 - *Fourth order in the power series expansion (in fs^4)*

  Create a fourth order polynomial phase.

The phase transfer function of the Dazzler is modeled by the following formula [17]:

$$\phi_{Dazzler}(\omega) = -(a_1(\omega - \omega_0) + \frac{a_2}{2}(\omega - \omega_0)^2 + \frac{a_3}{6}(\omega - \omega_0)^3 + \frac{a_4}{24}(\omega - \omega_0)^4) \qquad \text{(B.5)}$$

The output phase $\phi_{out}(\omega)$ is then obtained by adding the Dazzler induced phase to the phase of the input pulse:

$$\phi_{out}(\omega) = \phi_{in}(\omega) + \phi_{Dazzler}(\omega) \qquad \text{(B.6)}$$

B.4 Output Pulse

This gold area shows the output pulse in time domain and its spectral amplitude and spectral phase.
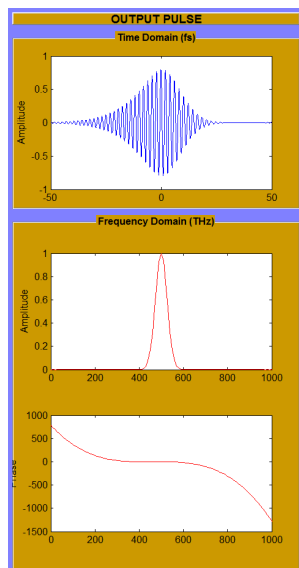
Figure B.5: Output Pulse area.

B.4.1 Time Domain (fs)

This panel provides a graphic view of the electric field of the output pulse in the time domain $E_{out}(t)$. It is calculated from the output spectral amplitude $A_{out}(\omega)$ and output spectral phase $\phi_{out}(\omega)$.

By default, $A_{out}(\omega) = A_{in}(\omega)$ and $\phi_{out}(\omega) = \phi_{in}(\omega)$, hence $E_{out}(t) = E_{in}(t)$.

If the Dazzler Control is used, then the spectral amplitude and/or spectral phase are shaped. See Sections B.3.1 and B.3.2 for the corresponding output spectral amplitude and output spectral phase.

The electric field of the output pulse in time domain is then provide by the Inverse Fast Fourier Transform (IFFT) of this expression:

$$E_{out}(\omega) = A_{out}(\omega).\mathrm{e}^{-i.\phi_{out}(\omega)} \tag{B.7}$$

B.4.2   Frequency Domain (THz)

This panel provides a graphic view of the spectral amplitude and spectral phase for the output pulse. By default, $A_{out}(\omega) = A_{in}(\omega)$ and $\phi_{out}(\omega) = \phi_{in}(\omega)$. If the Dazzler Control is used, then the spectral amplitude and/or spectral phase are shaped.

Appendix C

Dazzler™ modeling with Matlab™ - Source code

C.1   Program **MainPanel.m**

```matlab
%% Evolution of a Pulse through a Dazzler
% Jonathan Barreaux
% v1.0 / last modified 23/05/2012

clc
clear all

global tmax tres vmax vres fwhm lambda0 v0 panel3 panel4 panel5 panel6 panel7...
    a1 a2 a3 a4 holpos holwid holdep

tmax = 0;
tres = 0;
vmax = 0;
vres = 0;
fwhm = 0;
lambda0 = 0;
v0 = 0;
holpos = 0;
holwid = 0;
holdep = 0;
a1 = 0;
a2 = 0;
a3 = 0;
a4 = 0;

f1 = figure(1);
set(f1,'Units','normalized','Position',[0 0 1 1],'Toolbar','none',...
    'Name','Modeling of Pulse Shaping by a Dazzler v1.0',...
    'NumberTitle','off','Color',[0.5,0.5,1])

uicontrol('Parent',f1,'Units','normalized',...
    'Position',[0.843 0.982 0.2 0.018],'BackgroundColor',[0.5,0.5,1],...
    'Style','text','String','v1.0   Jonathan L.P. Barreaux, 2012');
```

```matlab
37  %%%%%%%%%%%%%
38  % INPUT PULSE %
39  %%%%%%%%%%%%%
40
41  %% Plotting Windows
42  uicontrol('Parent',f1,'Units','normalized',...
43      'Position',[0.03 0.94 0.335 0.022],'String','INPUT PULSE',...
44      'FontWeight','bold','FontSize',12,'BackgroundColor',[0.5,0.8,0]);
45
46  panel1 = uipanel('Parent',f1,'Units','normalized',...
47      'Position',[0.03 0.515 0.08 0.415],'BackgroundColor',[0.5,0.8,0],...
48      'Title','Pulse Parameters','TitlePosition','centertop',...
49      'FontWeight','bold','FontSize',10);
50  panel2 = uipanel('Parent',f1,'Units','normalized',...
51      'Position',[0.03 0.02 0.08 0.415],'BackgroundColor',[0.5,0.8,0],...
52      'Title','Plot Parameters','TitlePosition','centertop',...
53      'FontWeight','bold','FontSize',10);
54  panel3 = uipanel('Parent',f1,'Units','normalized',...
55      'Position',[0.12 0.63 0.245 0.30],'BackgroundColor',[0.5,0.8,0],...
56      'Title','Time Domain (fs)','TitlePosition','centertop',...
57      'FontWeight','bold','FontSize',10);
58  panel4 = uipanel('Parent',f1,'Units','normalized',...
59      'Position',[0.12 0.02 0.245 0.60],'BackgroundColor',[0.5,0.8,0],...
60      'Title','Frequency Domain (THz)','TitlePosition','centertop',...
61      'FontWeight','bold','FontSize',10);
62
63  subplot(1,1,1,'Parent',panel3)
64  ylabel('Amplitude')
65
66  subplot(2,1,1,'Parent',panel4)
67  ylabel('Magnitude')
68
69  subplot(2,1,2,'Parent',panel4)
70  ylabel('Phase')
71
72
73  %% Pulse Parameters
74  LAMBDA0 = uipanel('Parent',panel1,'Units','normalized',...
75      'Position',[0.02 0.77 0.96 0.15],'Title','Wavelength (nm)',...
76      'TitlePosition','centertop','FontWeight','bold',...
77      'backgroundcolor',[0.7 0.7 0.7]);
78  Valeur_lambda0 = uicontrol('Parent',LAMBDA0,'Units','normalized',...
79      'Position',[0.25 0.25 0.5 0.5],'Style','edit',...
80      'String',num2str(lambda0*1e9));
81
82  V0 = uipanel('Parent',panel1,'Units','normalized',...
83      'Position',[0.02 0.54 0.96 0.15],'Title','Frequency (THz)',...
84      'TitlePosition','centertop','FontWeight','bold',...
85      'backgroundcolor',[0.7 0.7 0.7]);
86  Valeur_v0 = uicontrol('Parent',V0,'Units','normalized',...
87      'Position',[0.25 0.25 0.5 0.5],'Style','text','FontWeight','bold',...
88      'String',num2str(v0*1e-12),'backgroundcolor',[0.7 0.7 0.7]);
89
90  FWHM = uipanel('Parent',panel1,'Units','normalized',...
91      'Position',[0.02 0.31 0.96 0.15],'Title','Pulse Width (fs)',...
92      'TitlePosition','centertop','FontWeight','bold',...
93      'backgroundcolor',[0.7 0.7 0.7]);
94  Valeur_fwhm = uicontrol('Parent',FWHM,'Units','normalized',...
95      'Position',[0.25 0.25 0.5 0.5],'Style','edit',...
96      'String',num2str(fwhm*1e15));
```

```matlab
97
98  PULSHA = uipanel('Parent',panel1,'Units','normalized',...
99      'Position',[0.02 0.08 0.96 0.15],'Title','Pulse Shape',...
100     'TitlePosition','centertop','FontWeight','bold',...
101     'backgroundcolor',[0.7 0.7 0.7]);
102 Valeur_PulSha = uicontrol('Parent',PULSHA,'Units','normalized',...
103     'Position',[0.05 0.2 0.9 0.6],'Style','popupmenu',...
104     'String',{'Gaussian Pulse','Sech Pulse'});
105
106
107 %% Plot Parameters
108 TMAX = uipanel('Parent',panel2,'Units','normalized',...
109     'Position',[0.02 0.77 0.96 0.15],'Title','Time Window (fs)',...
110     'TitlePosition','centertop','FontWeight','bold',...
111     'backgroundcolor',[0.7 0.7 0.7]);
112 Valeur_tmax = uicontrol('Parent',TMAX,'Units','normalized',...
113     'Position',[0.25 0.25 0.5 0.5],'Style','edit',...
114     'String',num2str(tmax*1e15));
115
116 TRES = uipanel('Parent',panel2,'Units','normalized',...
117     'Position',[0.02 0.54 0.96 0.15],'Title','Time Resolution (fs)',...
118     'TitlePosition','centertop','FontWeight','bold',...
119     'backgroundcolor',[0.7 0.7 0.7]);
120 Valeur_tres = uicontrol('Parent',TRES,'Units','normalized',...
121     'Position',[0.25 0.25 0.5 0.5],'Style','edit',...
122     'String',num2str(tres*1e15));
123
124 VMAX = uipanel('Parent',panel2,'Units','normalized',...
125     'Position',[0.02 0.31 0.96 0.15],'Title','Freq. Window (THz)',...
126     'TitlePosition','centertop','FontWeight','bold',...
127     'backgroundcolor',[0.7 0.7 0.7]);
128 Valeur_vmax = uicontrol('Parent',VMAX,'Units','normalized',...
129     'Position',[0.25 0.25 0.5 0.5],'Style','text','FontWeight','bold',...
130     'String',num2str(vmax*1e-12),'backgroundcolor',[0.7 0.7 0.7]);
131
132 VRES = uipanel('Parent',panel2,'Units','normalized',...
133     'Position',[0.02 0.08 0.96 0.15],'Title','Freq. Resolution (THz)',...
134     'TitlePosition','centertop','FontWeight','bold',...
135     'backgroundcolor',[0.7 0.7 0.7]);
136 Valeur_vres = uicontrol('Parent',VRES,'Units','normalized',...
137     'Position',[0.25 0.25 0.5 0.5],'Style','text','FontWeight','bold',...
138     'String',num2str(vres*1e-12),'backgroundcolor',[0.7 0.7 0.7]);
139
140
141
142 %%%%%%%%%%%%%%%%%
143 % MESSAGE WINDOW %
144 %%%%%%%%%%%%%%%%%
145 uicontrol('Parent',f1,'Units','normalized',...
146     'Position',[0.4005 0.94 0.29 0.022],'String','MESSAGE WINDOW',...
147     'FontWeight','bold','FontSize',12,'BackgroundColor',[0.6,0.6,0.6]);
148
149 panel7 = uipanel('Parent',f1,'Units','normalized',...
150     'Position',[0.4 0.60 0.29 0.33],'BackgroundColor',[0.6,0.6,0.6]);
151
152 uicontrol('Parent',panel7,'Units','normalized','Position',[0.01 0.5 0.98 0.05],
            ...
153         'Style','text','FontWeight','bold','backgroundcolor',[0.4,0.9,1],...
154         'String','WELCOME IN THIS DAZZLER MODELING PROGRAMME');
155
```

```matlab
156
157
158  %%%%%%%%%%%%%%%%%%
159  % DAZZLER CONTROL %
160  %%%%%%%%%%%%%%%%%%
161
162  %% Plotting Windows
163  uicontrol('Parent',f1,'Units','normalized',...
164      'Position',[0.4 0.5575 0.29 0.022],'String','DAZZLER CONTROL',...
165      'FontWeight','bold','FontSize',12,'BackgroundColor',[1,0.4,0]);
166
167  panel8 = uipanel('Parent',f1,'Units','normalized',...
168      'Position',[0.4 0.3325 0.29 0.215],'BackgroundColor',[1,0.4,0],...
169      'Title','Amplitude Control','TitlePosition','centertop',...
170      'FontWeight','bold','FontSize',10);
171  panel9 = uipanel('Parent',f1,'Units','normalized',...
172      'Position',[0.4 0.0475 0.29 0.275],'BackgroundColor',[1,0.4,0],...
173      'Title','Phase Control','TitlePosition','centertop',...
174      'FontWeight','bold','FontSize',10);
175
176
177  %% Amplitude Control
178  HOLPOS = uipanel('Parent',panel8,'Units','normalized',...
179      'Position',[0.07 0.543 0.24 0.28],'Title','Hole Position (nm)',...
180      'TitlePosition','centertop','FontWeight','bold',...
181      'backgroundcolor',[0.7 0.7 0.7]);
182  Valeur_holpos = uicontrol('Parent',HOLPOS,'Units','normalized',...
183      'Position',[0.25 0.25 0.5 0.5],'Style','edit',...
184      'String',num2str(holpos*1e9));
185
186  HOLWID = uipanel('Parent',panel8,'Units','normalized',...
187      'Position',[0.38 0.543 0.24 0.28],'Title','Hole Width (nm)',...
188      'TitlePosition','centertop','FontWeight','bold',...
189      'backgroundcolor',[0.7 0.7 0.7]);
190  Valeur_holwid = uicontrol('Parent',HOLWID,'Units','normalized',...
191      'Position',[0.25 0.25 0.5 0.5],'Style','edit',...
192      'String',num2str(holwid*1e9));
193
194  HOLDEP = uipanel('Parent',panel8,'Units','normalized',...
195      'Position',[0.69 0.543 0.24 0.28],'Title','Hole Depth',...
196      'TitlePosition','centertop','FontWeight','bold',...
197      'backgroundcolor',[0.7 0.7 0.7]);
198  Valeur_holdep = uicontrol('Parent',HOLDEP,'Units','normalized',...
199      'Position',[0.25 0.25 0.5 0.5],'Style','edit',...
200      'String',num2str(holdep));
201
202
203  %% Phase Control
204  A1 = uipanel('Parent',panel9,'Units','normalized',...
205      'Position',[0.15 0.7 0.3 0.2],'Title','Delay (fs)',...
206      'TitlePosition','centertop','FontWeight','bold',...
207      'backgroundcolor',[0.7 0.7 0.7]);
208  Valeur_a1 = uicontrol('Parent',A1,'Units','normalized',...
209      'Position',[0.25 0.25 0.5 0.5],'Style','edit',...
210      'String',num2str(a1*1e15));
211
212  A2 = uipanel('Parent',panel9,'Units','normalized',...
213      'Position',[0.55 0.7 0.3 0.2],'Title','Second Order (fs^2)',...
214      'TitlePosition','centertop','FontWeight','bold',...
215      'backgroundcolor',[0.7 0.7 0.7]);
```

```matlab
216  Valeur_a2 = uicontrol('Parent',A2,'Units','normalized',...
217      'Position',[0.25 0.25 0.5 0.5],'Style','edit',...
218      'String',num2str(a2*1e30));
219
220  A3 = uipanel('Parent',panel9,'Units','normalized',...
221      'Position',[0.15 0.4 0.3 0.2],'Title','Third Order (fs^3)',...
222      'TitlePosition','centertop','FontWeight','bold',...
223      'backgroundcolor',[0.7 0.7 0.7]);
224  Valeur_a3 = uicontrol('Parent',A3,'Units','normalized',...
225      'Position',[0.25 0.25 0.5 0.5],'Style','edit',...
226      'String',num2str(a3*1e45));
227
228  A4 = uipanel('Parent',panel9,'Units','normalized',...
229      'Position',[0.55 0.4 0.3 0.2],'Title','Fourth Order (fs^4)',...
230      'TitlePosition','centertop','FontWeight','bold',...
231      'backgroundcolor',[0.7 0.7 0.7]);
232  Valeur_a4 = uicontrol('Parent',A4,'Units','normalized',...
233      'Position',[0.25 0.25 0.5 0.5],'Style','edit',...
234      'String',num2str(a4*1e60));
235
236
237
238  %%%%%%%%%%%%%%
239  % OUTPUT PULSE %
240  %%%%%%%%%%%%%%%%
241
242  %% Plotting Windows
243  uicontrol('Parent',f1,'Units','normalized',...
244      'Position',[0.725 0.94 0.245 0.022],'String','OUTPUT PULSE',...
245      'FontWeight','bold','FontSize',12,'BackgroundColor',[0.8,0.6,0]);
246
247  panel5 = uipanel('Parent',f1,'Units','normalized',...
248      'Position',[0.725 0.63 0.245 0.30],'BackgroundColor',[0.8,0.6,0],...
249      'Title','Time Domain (fs)','TitlePosition','centertop',...
250      'FontWeight','bold','FontSize',10);
251  panel6 = uipanel('Parent',f1,'Units','normalized',...
252      'Position',[0.725 0.02 0.245 0.60],'BackgroundColor',[0.8,0.6,0],...
253      'Title','Frequency Domain (THz)','TitlePosition','centertop',...
254      'FontWeight','bold','FontSize',10);
255
256  subplot(1,1,1,'Parent',panel5)
257  ylabel('Amplitude')
258
259  subplot(2,1,1,'Parent',panel6)
260  ylabel('Magnitude')
261
262  subplot(2,1,2,'Parent',panel6)
263  ylabel('Phase')
264
265
266
267  %%%%%%%%%%%%%%%%%%%%%%%%%%
268  % VALIDATION PUSHBUTTONS %
269  %%%%%%%%%%%%%%%%%%%%%%%%%%
270
271  V = {@PulseCalculation,Valeur_lambda0,Valeur_v0,Valeur_fwhm,Valeur_PulSha,...
272      Valeur_tmax,Valeur_tres,Valeur_vmax,Valeur_vres,...
273      Valeur_a1,Valeur_a2,Valeur_a3,Valeur_a4,...
274      Valeur_holpos,Valeur_holwid,Valeur_holdep};
275
```

```
276  Valid_input = uicontrol('Parent',f1,'Units','normalized',...
277      'Position',[0.03 0.455 0.08 0.04],'Style','pushbutton','String','OK',...
278      'Callback',V);
279
280  Valid_ampli = uicontrol('Parent',panel8,'Units','normalized',...
281      'Position',[0.35 0.197 0.3 0.19],'Style','pushbutton','String','OK',...
282      'Callback',V);
283
284  Valid_phase = uicontrol('Parent',panel9,'Units','normalized',...
285      'Position',[0.35 0.125 0.3 0.15],'Style','pushbutton','String','OK',...
286      'Callback',V);
```

C.2   Program **PulseCalculation.m**

```
1   function PulseCalculation(hobject,eventdata,Valeur_lambda0,Valeur_v0,Valeur_fwhm
        ,...
2       Valeur_PulSha,Valeur_tmax,Valeur_tres,Valeur_vmax,Valeur_vres,...
3       Valeur_a1,Valeur_a2,Valeur_a3,Valeur_a4,...
4       Valeur_holpos,Valeur_holwid,Valeur_holdep)
5
6       global tmax tres vmax vres fwhm lambda0 v0 panel3 panel4 panel5 panel6
            panel7...
7       a1 a2 a3 a4 holpos holwid holdep
8
9
10
11  %%%%%%%%%%%%%%%%
12  % MESSAGE WINDOW %
13  %%%%%%%%%%%%%%%%%
14  delete(get(panel7,'Children'));  %Clean Message Window
15  err = 0.9;  %Set index for messages
16
17
18
19  %%%%%%%%%%%%%
20  % INPUT PULSE %
21  %%%%%%%%%%%%%
22
23  %% Pulse Parameters
24  lambda0 = sscanf(get(Valeur_lambda0,'String'),'%f')*1e-9;  %Wavelength
25  fwhm = sscanf(get(Valeur_fwhm,'String'),'%f')*1e-15;  %Pulse FWHM in intensity
26
27  if (¬isscalar(lambda0) || lambda0≤0)
28      lambda0 = 0;
29      uicontrol('Parent',panel7,'Units','normalized','Position',[0.01 err 0.98 0
            .05],...
30          'Style','text','FontWeight','bold','backgroundcolor',[0.5,0.8,0],...
31          'String','ERROR in Pulse Parameters >>> Wavelength must be a nonzero
                positive scalar!');
32      err = err-0.1;
33  end
34  if (¬isscalar(fwhm) || fwhm≤0)
35      fwhm = 0;
36      uicontrol('Parent',panel7,'Units','normalized','Position',[0.01 err 0.98 0
            .05],...
37          'Style','text','FontWeight','bold','backgroundcolor',[0.5,0.8,0],...
38          'String','ERROR in Pulse Parameters >>> Pulse FWHM must be a nonzero
                positive scalar!');
```

```matlab
39       err = err-0.1;
40   end
41
42   set(Valeur_lambda0,'String',num2str(lambda0*1e9));
43   set(Valeur_fwhm,'String',num2str(fwhm*1e15));
44
45   cl = 299792458;   %Celerity of light in vacuum
46   v0 = cl/lambda0;   %Light Frequency
47   set(Valeur_v0,'String',num2str(v0*1e-12));
48
49   w0 = 2*pi*v0;   %Angular Frequency
50   a = 2*log(2)/fwhm^2;
51   b = 0;   %Chirp Coefficient
52   gamma = a-1i*b;   %Complex Gaussian Parameter
53
54
55   %% Plot Parameters
56   tmax = sscanf(get(Valeur_tmax,'String'),'%f')*1e-15;   %Time Window
57   tres = sscanf(get(Valeur_tres,'String'),'%f')*1e-15;   %Time Resolution
58
59   if (¬isscalar(tmax) || tmax≤0)
60       tmax = 0;
61       uicontrol('Parent',panel7,'Units','normalized','Position',[0.01 err 0.98 0
               .05],...
62           'Style','text','FontWeight','bold','backgroundcolor',[0.5,0.8,0],...
63           'String','ERROR in Plot Parameters ⋙ Time Window must be a nonzero
                   positive scalar!');
64       err = err-0.1;
65   end
66   if (¬isscalar(tres) || tres≤0)
67       tres = 0;
68       uicontrol('Parent',panel7,'Units','normalized','Position',[0.01 err 0.98 0
               .05],...
69           'Style','text','FontWeight','bold','backgroundcolor',[0.5,0.8,0],...
70           'String','ERROR in Plot Parameters ⋙ Time Resolution must be a nonzero
                   positive scalar!');
71       err = err-0.1;
72   end
73
74   set(Valeur_tmax,'String',num2str(tmax*1e15));
75   set(Valeur_tres,'String',num2str(tres*1e15));
76
77   vmax = 2*v0;
78   set(Valeur_vmax,'String',num2str(vmax*1e-12));
79   vres = 1/tmax;
80   set(Valeur_vres,'String',num2str(vres*1e-12));
81
82   t = -tmax/2:tres:tmax/2;   %Temporal Scale
83   N = length(t);   %Number of points for the plot
84   v = (1/tres)*linspace(0,1,N);   %Frequency Scale
85
86
87   %% Input Electric Field in Temporal Domain
88   if (tmax≠0 && tres≠0 && fwhm≠0 && lambda0≠0)
89       PulSha = get(Valeur_PulSha,'Value');   %Pulse Shape
90
91       for m = 1:N
92           if PulSha == 1
93               Et1_plot(m) = exp(-gamma*t(m)^2+1i*w0*t(m));   %Gaussian Pulse
94           else
```

```matlab
95              Et1_plot(m) = sech(t(m)*1.76/fwhm)*exp(1i*(w0*t(m)+b*t(m)^2)); %Sech
                     Pulse
96          end
97      end
98
99      Et1 = [Et1_plot((N+1)/2:N) Et1_plot(1:(N-1)/2)];
100
101     subplot(1,1,1,'Parent',panel3)
102     plot(t*1e15,real(Et1_plot))
103     ylabel('Amplitude')
104     axis([-tmax*1e15/2 tmax*1e15/2 -1 1])
105 end
106
107
108 %% FFT: Input Amplitude and Phase in Frequency Domain
109 if (tmax≠0 && tres≠0 && fwhm≠0 && lambda0≠0)
110     Ev1 = fft(Et1);   %FFT of the Input Electric Field
111     AmpEv1 = abs(Ev1);  %Amplitude of the Input Electric Field in Frequency
            Domain
112     PhaEv1 = unwrap(angle(Ev1));  %Phase of the Input Electric Field in
            Frequency Domain
113
114     subplot(2,1,1,'Parent',panel4)
115     plot(v/1e12,AmpEv1/max(AmpEv1),'Color','red')
116     ylabel('Amplitude')
117     axis([0 2*v0/1e12 0 1])
118
119     subplot(2,1,2,'Parent',panel4)
120     plot(v/1e12,PhaEv1,'Color','red')
121     ylabel('Phase')
122     xlim([0 2*v0/1e12])
123 end
124
125
126 if (err≠0.9 || tmax==0 || tres==0 || fwhm==0 || lambda0==0)
127     uicontrol('Parent',panel7,'Units','normalized','Position',[0.01 err 0.98 0
            .05],...
128         'Style','text','FontWeight','bold','backgroundcolor',[0.4,0.9,1],...
129         'String','ERROR(S) in Input Pulse >>> Plotting cancelled!');
130     err = err-0.1;
131 else
132     uicontrol('Parent',panel7,'Units','normalized','Position',[0.01 err 0.98 0
            .05],...
133         'Style','text','FontWeight','bold','backgroundcolor',[0.4,0.9,1],...
134         'String','Input Pulse >>> Plotting done!');
135     err = err-0.1;
136 end
137
138
139
140 %%%%%%%%%%%%%%%%%
141 % DAZZLER CONTROL %
142 %%%%%%%%%%%%%%%%%%%
143
144 %% Amplitude Parameters Gathering
145 holpos = sscanf(get(Valeur_holpos,'String'),'%f')*1e-9;  %Hole Position
146 holwid = sscanf(get(Valeur_holwid,'String'),'%f')*1e-9;  %Hole Width
147 holdep = sscanf(get(Valeur_holdep,'String'),'%f');  %Hole Depth
148
149 if (¬isscalar(holpos) || holpos<0)
```

```matlab
150     holpos = 0;
151     uicontrol('Parent',panel7,'Units','normalized','Position',[0.01 err 0.98 0
                .05],...
152         'Style','text','FontWeight','bold','backgroundcolor',[1,0.4,0],...
153         'String','ERROR in Amplitude Control >>> Hole Position must be a
                    positive scalar!');
154     err = err-0.1;
155 end
156 if (¬isscalar(holwid) || holwid<0)
157     holwid = 0;
158     uicontrol('Parent',panel7,'Units','normalized','Position',[0.01 err 0.98 0
                .05],...
159         'Style','text','FontWeight','bold','backgroundcolor',[1,0.4,0],...
160         'String','ERROR in Amplitude Control >>> Hole Width must be a positive
                    scalar!');
161     err = err-0.1;
162 end
163 if (¬isscalar(holdep) || holdep<0 || holdep>1)
164     holdep = 0;
165     uicontrol('Parent',panel7,'Units','normalized','Position',[0.01 err 0.98 0
                .05],...
166         'Style','text','FontWeight','bold','backgroundcolor',[1,0.4,0],...
167         'String','ERROR in Amplitude Control >>> Hole Depth must be a scalar
                    between 0 and 1!');
168     err = err-0.1;
169 end
170
171 set(Valeur_holpos,'String',num2str(holpos*1e9));
172 set(Valeur_holwid,'String',num2str(holwid*1e9));
173 set(Valeur_holdep,'String',num2str(holdep));
174
175
176 %% Useful Parameters
177 if (holpos≠0 && holwid≠0 && holdep≠0)
178     w1 = 2*pi*cl/holpos;
179     khi1 = holwid/(2*holpos);
180     dw1 = w1*(khi1-(khi1^3))/2;
181 end
182
183
184 %% Phase Parameters Gathering
185 a1 = sscanf(get(Valeur_a1,'String'),'%f')*1e-15;   %Delay
186 a2 = sscanf(get(Valeur_a2,'String'),'%f')*1e-30;   %Second Order
187 a3 = sscanf(get(Valeur_a3,'String'),'%f')*1e-45;   %Third Order
188 a4 = sscanf(get(Valeur_a4,'String'),'%f')*1e-60;   %Fourth Order
189
190 if (¬isscalar(a1))
191     a1 = 0;
192     uicontrol('Parent',panel7,'Units','normalized','Position',[0.01 err 0.98 0
                .05],...
193         'Style','text','FontWeight','bold','backgroundcolor',[1,0.4,0],...
194         'String','ERROR in Phase Control >>> Delay is not a scalar!');
195     err = err-0.1;
196 end
197 if (¬isscalar(a2))
198     a2 = 0;
199     uicontrol('Parent',panel7,'Units','normalized','Position',[0.01 err 0.98 0
                .05],...
200         'Style','text','FontWeight','bold','backgroundcolor',[1,0.4,0],...
201         'String','ERROR in Phase Control >>> Second Order is not a scalar!');
```

```matlab
202        err = err-0.1;
203    end
204    if (¬isscalar(a3))
205        a3 = 0;
206        uicontrol('Parent',panel7,'Units','normalized','Position',[0.01 err 0.98 0
               .05],...
207            'Style','text','FontWeight','bold','backgroundcolor',[1,0.4,0],...
208            'String','ERROR in Phase Control ⋙ Third Order is not a scalar!');
209        err = err-0.1;
210    end
211    if (¬isscalar(a4))
212        a4 = 0;
213        uicontrol('Parent',panel7,'Units','normalized','Position',[0.01 err 0.98 0
               .05],...
214            'Style','text','FontWeight','bold','backgroundcolor',[1,0.4,0],...
215            'String','ERROR in Phase Control ⋙ Fourth Order is not a scalar!');
216        err = err-0.1;
217    end
218
219    set(Valeur_a1,'String',num2str(a1*1e15));
220    set(Valeur_a2,'String',num2str(a2*1e30));
221    set(Valeur_a3,'String',num2str(a3*1e45));
222    set(Valeur_a4,'String',num2str(a4*1e60));
223
224
225
226    %%%%%%%%%%%%%%
227    % OUTPUT PULSE %
228    %%%%%%%%%%%%%%%
229
230    %% Modificated Output Amplitude and Phase in Frequency Domain
231    if (tmax≠0 && tres≠0 && fwhm≠0 && lambda0≠0)
232        if (holpos≠0 && holwid≠0 && holdep≠0)
233            for m = 1:N
234                gamp(m) = 1 - holdep*exp(-((2*pi*v(m)-w1)/dw1)^2);
235                AmpEv2(m) = AmpEv1(m)*gamp(m);
236            end
237        else
238            AmpEv2 = AmpEv1;
239        end
240
241        for m = 1:N
242            PhaEv2(m) = -(a1*(2*pi*v(m)-w0)+(a2/2)*(2*pi*v(m)-w0)^2 +...
243                (a3/6)*(2*pi*v(m)-w0)^3+(a4/24)*(2*pi*v(m)-w0)^4) + PhaEv1(m);
244        end
245
246        subplot(2,1,1,'Parent',panel6)
247        plot(v/1e12,AmpEv2/max(AmpEv1),'Color','red')
248        ylabel('Amplitude')
249        axis([0 2*v0/1e12 0 1])
250
251        subplot(2,1,2,'Parent',panel6)
252        plot(v/1e12,PhaEv2,'Color','red')
253        ylabel('Phase')
254        xlim([0 2*v0/1e12])
255    end
256
257
258    %% IFFT: Output Electric Field in Temporal Domain
259    if (tmax≠0 && tres≠0 && fwhm≠0 && lambda0≠0)
```

```matlab
260        for m = 1:N
261            Ev2(m) = AmpEv2(m)*exp(-1i*PhaEv2(m));
262        end
263
264        Et2 = ifft(Ev2);
265
266        Et2_plot = [Et2((N+1)/2:N) Et2(1:(N-1)/2)];
267
268
269        subplot(1,1,1,'Parent',panel5)
270        plot(t*1e15,real(Et2_plot))
271        ylabel('Amplitude')
272        axis([-tmax/2*1e15 tmax/2*1e15 -1 1])
273    end
274
275    if (err≠0.8 || tmax==0 || tres==0 || fwhm==0 || lambda0==0)
276        uicontrol('Parent',panel7,'Units','normalized','Position',[0.01 err 0.98 0
                .05],...
277            'Style','text','FontWeight','bold','backgroundcolor',[0.4,0.9,1],...
278            'String','ERROR(S) in Output Pulse >>> Plotting cancelled!');
279        err = err-0.1;
280    else
281        uicontrol('Parent',panel7,'Units','normalized','Position',[0.01 err 0.98 0
                .05],...
282            'Style','text','FontWeight','bold','backgroundcolor',[0.4,0.9,1],...
283            'String','Output Pulse >>> Plotting done!');
284        err = err-0.1;
285    end
286
287
288    end
```

Bibliography

[1] C. Winterfeldt, *Generation and control of high-harmonic radiation*. PhD thesis, Universität Würzburg, 2006.

[2] M. W. Hendrikx, "High harmonic generation in gas-filled capillary waveguides," Master's thesis, University of Twente, 2009.

[3] B.-J. Zandt, "Towards effcient high harmonic generation in the few nm wavelength regime," Master's thesis, University of Twente, 2009.

[4] P. B. Corkum, "Plasma perspective on strong field multiphoton ionization," *Physical Review Letters*, vol. 71, pp. 1994–1997, 1993.

[5] M. Lewenstein, P. Balcou, M. Y. Ivanov, A. L'Huillier, and P. B. Corkum, "Theory of high-harmonic generation by low-frequency laser fields," *Physical Review A*, vol. 49, pp. 2117–2132, March 1994.

[6] A. D. Shiner, C. Trallero-Herrero, N. Kajumba, H.-C. Bandulet, D. Comtois, F. Légaré, M. Giguère, J.-C. Kieffer, P. B. Corkum, and D. M. Villeneuve, "Wavelength scaling of high harmonic generation efficiency," *Physical Review Letters*, vol. 103, August 2009.

[7] A. Rundquist, C. G. Durfee, Z. Chang, C. Herne, S. Backus, M. M. Murnane, and H. C. Kapteyn, "Phase-matched generation of coherent soft x-ray," *Science*, vol. 280, no. 1412, 1998.

[8] E. A. Gibson, *Quasi-phase matching of soft X-ray light from high-order harmonic generation using waveguide structures*. PhD thesis, University of Colorado, 2004.

[9] T. Popmintchev, M.-C. Chen, P. Arpin, M. M. Murnane, and H. C. Kapteyn, "The attosecond nonlinear optics of bright coherent x-ray generation," *Nature Photonics*, vol. 4, pp. 822–832, 2010.

[10] Coherent, *Mantis Laser Operator's Manual*, September 2008.

[11] Coherent, *Legend Elite Operator's Manual*, November 2009.

[12] P. Tournois, "Acousto-optic programmable dispersive filter for adaptive compensation of group delay time dispersion in laser systems," *Optics Communications*, vol. 140, pp. 245–249, 1997.

[13] D. Kaplan and P. Tournois, "Theory and performance of the acousto-optic programmable dispersive filter used for femtosecond laser pulse shaping," *Journal de Physique IV*, vol. 12, June 2002.

[14] F. Verluise, V. Laude, Z. Cheng, C. Spielmann, and P. Tournois, "Amplitude and phase control of ultrashort pulses by use of an acousto-optic programmable dispersive filter: pulse compression and shaping," *Optics Letters*, vol. 25, April 2000.

[15] T. Oksenhendler, P. Rousseau, R. Herzog, O. Gobert, M. Perdrix, and P. Meynadier, "20Hz Femtosecond laser amplifier optimization using an AOPDF pulse shaper and a SPIDER," in *Conference on Lasers and Electro-Optics (CLEO)*, pp. 1176–1177, June 2003.

[16] A. E. Siegman, *Lasers*. University Science Books, 1986.

[17] Fastlite, *Dazzler System Computation Process*, 2006.

[18] M. Born and E. Wolf, *Principles of Optics*. Cambridge University Press, October 1999.

[19] W. Postma, "Measurement of femtosecond pulses with an autocorrelator and a Grenouille FROG," Master's thesis, University of Twente, 2008.

Abstract

High-harmonic generation (HHG) is an extreme nonlinear optical process that allows the conversion of infrared laser light into coherent radiation with shorter wavelengths, in the extreme ultraviolet or soft X-ray regime (1-100 nm).

Sources based on high-harmonic generation hold unique promises for application in diffractive imaging of single molecules and the seeding of free electron lasers (FEL), exploiting specifically the coherent nature and the short wavelength of the harmonic radiation.

The tuning and the enhancement of the high-harmonic generation will be of great use. Indeed high-harmonic generation only produces odd harmonics of the fundamental frequency. For instance, for the seeding of a free electron lasers, it could necessary to tune these harmonics in order to fit one of them with the spectral gain area of the free electron lasers. The enhancement could then be used to increase the power of the harmonic fitting with the spectral gain area, to the detriment of the other harmonics. These are made by inducing modifications on the spectrum of the drive electric field used to produce high-harmonic generation.

This report describes trials of tuning and enhancement of high-harmonic generation produced in a gas-filled hollow waveguide, using a device called Dazzler, brand name of the acousto-optic programmable dispersive filter (AO-PDF) developed by Pierre Tournois.